INSTITUTE OF PHYSICS PUBLISHING PHYSICS IN MEDICINE AND BIOLOGY

Phys. Med. Biol. **47** (2002) 523–555 PII: S0031-9155(02)27491-6

On MEG forward modelling using multipolar expansions

K Jerbi[1,2], J C Mosher[3], S Baillet[2] and R M Leahy[1]

[1] Signal and Image Processing Institute, University of Southern California, Los Angeles, CA, USA
[2] Cognitive Neuroscience and Brain Imaging Laboratory, Hôpital de la Salpêtière, CNRS, Paris, France
[3] Los Alamos National Laboratory, Los Alamos, NM, USA

E-mail: leahy@sipi.usc.edu

Received 2 August 2001
Published 1 February 2002
Online at stacks.iop.org/PMB/47/523

Abstract

Magnetoencephalography (MEG) is a non-invasive functional imaging modality based on the measurement of the external magnetic field produced by neural current sources within the brain. The reconstruction of the underlying sources is a severely ill-posed inverse problem typically tackled using either low-dimensional parametric source models, such as an equivalent current dipole (ECD), or high-dimensional minimum-norm imaging techniques. The inability of the ECD to properly represent non-focal sources and the over-smoothed solutions obtained by minimum-norm methods underline the need for an alternative approach. Multipole expansion methods have the advantages of the parametric approach while at the same time adequately describing sources with significant spatial extent and arbitrary activation patterns. In this paper we first present a comparative review of spherical harmonic and Cartesian multipole expansion methods that can be used in MEG. The equations are given for the general case of arbitrary conductors and realistic sensor configurations and also for the special cases of spherically symmetric conductors and radially oriented sensors. We then report the results of computer simulations used to investigate the ability of a first-order multipole model (dipole and quadrupole) to represent spatially extended sources, which are simulated by 2D and 3D clusters of elemental dipoles. The overall field of a cluster is analysed using singular value decomposition and compared to the unit fields of a multipole, centred in the middle of the cluster, using subspace correlation metrics. Our results demonstrate the superior utility of the multipolar source model over ECD models in providing source representations of extended regions of activity.

1. Introduction

Magnetoencephalography (MEG) is a non-invasive functional imaging modality based on the measurement of the external magnetic field produced by neural current sources within the human brain. MEG directly measures these electrophysiological signals with millisecond resolution. Because of this unique advantage over slower haemodynamic-based modalities, such as fMRI and PET, MEG is expected to play an important role in revealing crucial aspects of brain function and dysfunction. Unfortunately, MEG source estimation is a severely ill-posed inverse problem. Most approaches used to solve this problem can be roughly classified as either imaging or parametric methods. Imaging relies on a tessellation of the cortex, assigning an elemental current source to each area element, and solving the resulting linear inverse problem (Wang *et al* 1992). Accurate tessellations produce a highly underdetermined problem, the regularization of which leads to over-smoothed current distributions. An alternative approach is to use a parametric representation of the neural source. Such model-based methods include the classic equivalent current dipole (ECD) and its extension to multiple current dipole models (e.g. de Munck *et al* 1988, Mosher *et al* 1992, Hämäläinen *et al* 1993). The definition of these models is based on the assumption that the underlying sources can be adequately represented by the ECD. Although the ECD model can lead to accurate localization for very focal sources, localization error may increase in the case of spatially extended sources.

The ECD model generally oversimplifies the inverse problem, while the imaging methods tend to overly smooth the reconstructed source distributions. We consider here an alternative multipolar modelling approach that has the advantages of the parametric approach, in terms of a relatively small number of parameters to be estimated, while at the same time allowing for sources with significant spatial extent and arbitrary activation patterns.

The use of multipole expansions to solve biomagnetic inverse problems has mainly been restricted to magnetocardiography (MCG) (Grynszpan and Geselowitz 1973, Karp *et al* 1980, Katila and Karp 1983, Ernè *et al* 1988, Gonnelli and Agnello 1987, Nenonen *et al* 1991); however, a few MEG multipole source localization algorithms have recently been suggested (Alvarez 1991, Nolte and Curio 1997, 2000, Haberkorn 1998, Mosher *et al* 1999a, 1999b, 2000). Multipole expansions have also been used to tackle miscellaneous issues related to biomagnetic inverse problems other than direct source localization. For instance, spherical expansions may be used to achieve analytical descriptions of surface boundaries in realistic head models (Purcell *et al* 1991, Nolte *et al* 2001). The computation of higher order multipole moments can also be used to achieve a conversion of MCG recordings between separate acquisition systems (Burghoff *et al* 1997, 2000). Moreover, multipole expansion methods can be used to increase the accuracy of dust load estimation in the lungs (Stroink 1987).

The discussion in this paper is restricted to the application of multipoles to expand the magnetic field measured in MEG in order to improve localization precision and increase the information contained in the estimated source parameters. Our intentions in this paper are two-fold: (i) to present a comparative review of the different multipolar expansions that can be used in this context, and (ii) to investigate the utility of multipolar expansions in representing extended neural sources in MEG. In section 2, the general theory of multipole expansions is introduced. Section 3 describes the use of current multipole expansions (CME) to describe the MEG measurement field produced by a localized current source located at an arbitrary location within the spherical head model. Next, a magnetic multipole expansion (MME) framework for MEG is described in terms of spherical (section 4) and Cartesian (section 5) expansions. Section 6 investigates the field patterns generated by the current multipole expansion of the radial magnetic field and displays the results of computer simulations of patches and cubes of neural activity where singular value decompositions (SVD) and subspace correlation metrics

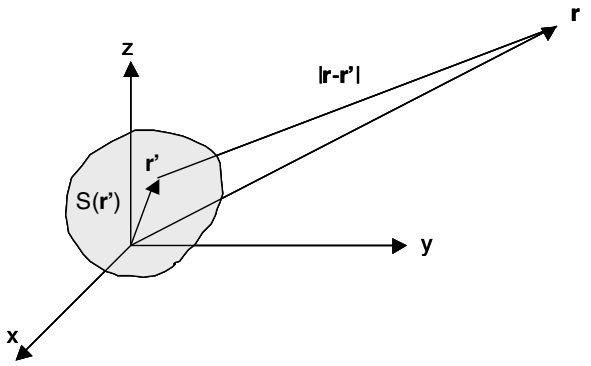

Figure 1. A localized source distribution $s(\boldsymbol{r}')$.

are used to investigate the ability of the multipolar source models to match the subspace spanned by clusters of elemental dipoles. Although important issues related to solving the inverse problem are briefly discussed at the end of the paper, the focus of this paper remains the forward mapping from neural sources to measured magnetic fields.

2. Multipole expansion methods

A multipole expansion is a series expansion that can be used to represent the field produced by a source in terms of an expansion parameter which becomes small as the distance from the source increases. The contributions of the leading terms in a multipole expansion are generally the strongest. Multipole expansions are commonly used in problems involving the gravitational field of mass aggregations, the electric and magnetic fields of charge and current distributions, and the propagation of electromagnetic waves. The objective of this section is to review the general properties of multipole expansions, a thorough understanding of which is a prerequisite to selecting a multipole expansion framework best suited to the MEG forward problem.

Consider Poisson's equation

$$\nabla^2\psi(\boldsymbol{r}) = -s(\boldsymbol{r}) \tag{1}$$

where $\boldsymbol{r}$ is the location vector and ψ is a scalar potential caused by a localized source distribution s, as illustrated in figure 1. The solution of (1) in integral form is

$$\psi(\boldsymbol{r}) = \frac{1}{4\pi}\int \frac{s(\boldsymbol{r}')}{|\boldsymbol{r}-\boldsymbol{r}'|}\,\mathrm{d}^3r' \tag{2}$$

where the integral must be evaluated over all regions where s is nonzero. If the source distribution s can be bounded by a closed surface S, then $\psi(\boldsymbol{r})$ outside S satisfies Laplace's equation. If the bounding surface is a sphere of radius a, for instance, we have

$$\nabla^2\psi(\boldsymbol{r}) = 0 \qquad r > a \tag{3}$$

where $r = |\boldsymbol{r}|$.

A multipole expansion of the scalar potential ψ outside the bounding surface can be achieved by expanding in spherical or Cartesian coordinates the Green's function

$$G(\boldsymbol{r}, \boldsymbol{r}') = \frac{1}{|\boldsymbol{r}-\boldsymbol{r}'|} \tag{4}$$

and inserting into (2). In the following we derive the multipole expansion by expanding the scalar Green's function using both spherical harmonic and Taylor series expansions.

2.1. The spherical harmonic multipole expansion

An expansion of the inverse of the distance between the observation point $\boldsymbol{r} = (\theta, \phi, r)$ and a source centred at $\boldsymbol{r}' = (\theta', \phi', r')$ is given by (Jackson 1975, p 92)

$$\frac{1}{|\boldsymbol{r} - \boldsymbol{r}'|} = \sum_{l=0}^{\infty} \frac{r'^l}{r^{l+1}} P_l(\cos\gamma) \qquad \text{for } r > r' \tag{5}$$

where $P_l(x)$ are the Legendre polynomials of order l and $\cos\gamma = (\boldsymbol{r} \cdot \boldsymbol{r}')/(rr')$, i.e. γ is the angle between $\boldsymbol{r}$ and $\boldsymbol{r}'$. The addition theorem for spherical harmonics is (Morse and Feshbach 1953)

$$P_l(\cos\gamma) = \frac{4\pi}{2l+1} \sum_{m=-l}^{l} \hat{Y}^*_{lm}(\theta', \phi') \hat{Y}_{lm}(\theta, \phi) \tag{6}$$

where the complex angular functions $\hat{Y}_{lm}$ are the normalized spherical harmonics

$$\hat{Y}_{lm}(\theta, \phi) = \sqrt{\frac{2l+1}{4\pi} \frac{(l-m)!}{(l+m)!}}\, P_l^m(\cos\theta)\, \mathrm{e}^{\mathrm{i}m\phi} \tag{7}$$

where $P_l^m(\cos\theta)$ are the associated Legendre functions of the first kind. We use the notation $\hat{Y}_{lm}$ to distinguish the above definition from the non-normalized spherical harmonics $Y_{lm} = P_l^m(\cos\theta)\, \mathrm{e}^{\mathrm{i}m\phi}$.

Inserting (6) in (5) yields an expansion of the scalar Green's function in spherical harmonics

$$\frac{1}{|\boldsymbol{r} - \boldsymbol{r}'|} = \sum_{l=0}^{\infty} \sum_{m=-l}^{l} \frac{4\pi}{2l+1} \frac{r'^l}{r^{l+1}} \hat{Y}^*_{lm}(\theta', \phi') \hat{Y}_{lm}(\theta, \phi) \tag{8}$$

from which we expand the potential ψ in (2) yielding

$$\psi(\boldsymbol{r}) = \sum_{l=0}^{\infty} \sum_{m=-l}^{l} \frac{1}{2l+1} A_{lm} \frac{\hat{Y}_{lm}(\theta, \phi)}{r^{l+1}} \tag{9}$$

where the complex coefficients A_{lm} are the *multipole moments* defined by

$$A_{lm} = \int \hat{Y}^*_{lm}(\theta', \phi')\, r'^l\, s(\boldsymbol{r}')\, \mathrm{d}^3 r'. \tag{10}$$

Hence the spherical harmonic multipole expansions provide a practical expression for computing the scalar potential ψ through a summation of rapidly decreasing terms ($\sim r'/r$) with an elegant separation of the observation parameters from the source parameters. The multipole moments A_{lm} fully describe the properties of the source distribution that can be inferred from the observations.

Note that some authors (e.g. Morse and Feshbach 1953, Wikswo and Swinney 1984) use the real form of the spherical expansions instead of the complex form given here.

2.2. The Cartesian multipole expansion

Instead of using spherical harmonics, an expansion in Cartesian coordinates can be achieved using a Taylor series expansion of the scalar Green's function about a location $\boldsymbol{l}$ yielding

$$\frac{1}{|\boldsymbol{r} - \boldsymbol{r}'|} = \sum_{n=0}^{\infty} \frac{1}{n!} [(\boldsymbol{r}' - \boldsymbol{l}) \cdot \nabla']^n \left(\frac{1}{|\boldsymbol{r} - \boldsymbol{r}'|} \right)_{r'=\boldsymbol{l}} \tag{11}$$

where ∇' is the gradient w.r.t. to the primed variables. The first terms of the Taylor series up to the order $n = 2$ provide a second-order approximation of Green's function

$$\frac{1}{|\boldsymbol{r}-\boldsymbol{r}'|} \simeq \frac{1}{|\boldsymbol{r}-\boldsymbol{l}|} + (\boldsymbol{r}'-\boldsymbol{l}) \cdot \left(\frac{\boldsymbol{r}-\boldsymbol{l}}{|\boldsymbol{r}-\boldsymbol{l}|^3}\right) + \frac{1}{2}(\boldsymbol{r}'-\boldsymbol{l})(\boldsymbol{r}'-\boldsymbol{l}) : \left(\frac{3(\boldsymbol{r}-\boldsymbol{l})(\boldsymbol{r}-\boldsymbol{l}) - \boldsymbol{I}|\boldsymbol{r}-\boldsymbol{l}|^2}{|\boldsymbol{r}-\boldsymbol{l}|^5}\right) \tag{12}$$

where the standard Cartesian tensor notation is used. The scalar product and the tensor contraction are defined by $\boldsymbol{A} \cdot \boldsymbol{B} = A_i B_i$ and $\boldsymbol{P} : \boldsymbol{Q} = P_{ij} Q_{ji}$, where i and j sum over x, y and z[4]. The unit tensor is denoted as $\boldsymbol{I}$, with elements $\boldsymbol{I}_{\alpha\beta} = \delta_{\alpha\beta}$ where $\delta_{\alpha\beta}$ is the Kronecker delta i.e. $\boldsymbol{I}$ is the 3×3 identity matrix.

The Taylor series expansion about the origin of the coordinate system, $\boldsymbol{l} = (0, 0, 0)$, simplifies by noting that $\nabla'(1/|\boldsymbol{r}-\boldsymbol{r}'|)|_{r'=0} = -\nabla(1/r)$, yielding

$$\frac{1}{|\boldsymbol{r}-\boldsymbol{r}'|} = \frac{1}{r} - \boldsymbol{r}' \cdot \nabla\left(\frac{1}{r}\right) + \frac{1}{2}\,\boldsymbol{r}'\boldsymbol{r}' : \nabla\nabla\left(\frac{1}{r}\right) + \cdots \tag{13}$$

$$= \frac{1}{r} + \boldsymbol{r}' \cdot \frac{\boldsymbol{r}}{r^3} + \frac{1}{2}\,\boldsymbol{r}'\boldsymbol{r}' : \left(\frac{3\,\boldsymbol{r}\boldsymbol{r} - \boldsymbol{I}\,r^2}{r^5}\right) + \cdots . \tag{14}$$

We will develop the Cartesian multipole expansion about the origin using (13), then generalize these results for an arbitrary expansion point $\boldsymbol{l}$. Inserting (13) in (2) gives (cf Wikswo and Swinney 1985)

$$\psi(\boldsymbol{r}) = \frac{1}{4\pi}\int s(\boldsymbol{r}')\,\mathrm{d}^3r'\left(\frac{1}{r}\right) - \frac{1}{4\pi}\int s(\boldsymbol{r}')\boldsymbol{r}'\,\mathrm{d}^3r' \cdot \nabla\left(\frac{1}{r}\right) + \frac{1}{4\pi}\,\frac{1}{2}\int s(\boldsymbol{r}')\boldsymbol{r}'\boldsymbol{r}'\,\mathrm{d}^3r' : \nabla\nabla\left(\frac{1}{r}\right) + \cdots . \tag{15}$$

The first three terms of the expansion represent the zeroth-, first-, and second-order multipole contributions to the overall potential at $\boldsymbol{r}$. The corresponding *monopole*, *dipole*, and *quadrupole* moments are given respectively by

$$\int s(\boldsymbol{r}')\,\mathrm{d}^3r' \qquad \int s(\boldsymbol{r}')\boldsymbol{r}'\,\mathrm{d}^3r' \qquad \frac{1}{2}\int s(\boldsymbol{r}')\boldsymbol{r}'\boldsymbol{r}'\,\mathrm{d}^3r'. \tag{16}$$

The Cartesian components of the dipole through octupole moments of the scalar multipole expansion, as well as simple source–sink configurations that help visualize them, are presented by Wikswo (1983).

A generalization of the procedure leads to an infinite Taylor series expansion about the origin (Morse and Feshbach 1953):

$$\psi(\boldsymbol{r}) = \frac{1}{4\pi}\sum_{n=0}^{\infty}\sum_{l=0}^{n}\sum_{k=0}^{n-l}\frac{(-1)^n}{l!k!(n-l-k)!}\,c_{nlk}\,\frac{\partial^n}{\partial x^l \partial y^k \partial z^{n-l-k}}\left(\frac{1}{r}\right) \tag{17}$$

where the nth-order multipole moments are

$$c_{nlk} = \int_{v'} s(\boldsymbol{r}')x'^l y'^k z'^{n-l-k}\,\mathrm{d}^3r'. \tag{18}$$

For completeness, we now consider a multipolar expansion of a vector potential $\boldsymbol{\Psi}(\boldsymbol{r})$ caused by a localized source vector $\boldsymbol{s}(\boldsymbol{r}')$. The solution of the related Poisson equation is

$$\Psi(\boldsymbol{r}) = \frac{1}{4\pi}\int \frac{\boldsymbol{s}(\boldsymbol{r}')}{|\boldsymbol{r}-\boldsymbol{r}'|}\,\mathrm{d}^3r'. \tag{19}$$

[4] Given four vectors $\boldsymbol{a}$, $\boldsymbol{b}$, $\boldsymbol{c}$ and $\boldsymbol{d}$, the colon product also satisfies $\boldsymbol{a}\boldsymbol{b} : \boldsymbol{c}\boldsymbol{d} = \boldsymbol{b} \cdot \boldsymbol{c}\boldsymbol{d} \cdot \boldsymbol{a}$.

By analogy to the scalar case, the expansion is achieved by expanding the dyadic Green's function $\boldsymbol{G}(\boldsymbol{r}, \boldsymbol{r}') = \boldsymbol{I}/|\boldsymbol{r} - \boldsymbol{r}'|$ where $\boldsymbol{I}$ is the unit dyadic. While expanding the dyadic Green's function in spherical harmonics leads to an elaborate expansion in terms of vector solutions of the vector Laplace equation (Morse and Feshbach 1953, p 1802), the expansion in Cartesian coordinates is less complex and can be easily derived by a straightforward extension of the equations for the scalar case replacing the scalar source term by its vector counterpart.

2.3. Comparison between spherical and Cartesian multipole expansions

Considerable algebraic manipulations can show that the *n*th order Cartesian multipole expansion is equivalent to the *n*th order spherical harmonic expansion. An important difference, however, is the number of moments in each expansion. The moments c_{nlk} in (18) show that the Taylor series multipole expansion up to an order n contains $(n+1)(n+2)/2$ moments. The spherical harmonics multipole expansion has only $(2n+1)$ moments given by A_{nm} in (10). The difference in the number of terms first appears for $n = 2$ for which the Taylor series expansion has six moments whereas the spherical harmonic series has only five.

The Taylor series has a redundant term which does not give rise to a potential. Morse and Feshbach (1953) note that this redundancy comes from the trace of the quadrupole tensor because the contribution of the unit dyadic results in a constant times $\nabla^2(1/r)$, which is zero. This degree of freedom is automatically neglected in the spherical harmonic series. A similar situations exists for the octupole. Three combinations of octupolar potentials from the Taylor expansion form silent distributions. Similar combinations also exist in higher order multipoles. Although the redundancy does not affect the utility of multipoles for describing an external potential, the redundancy can easily be avoided in the case of the quadrupole by forcing its tensor representation to be traceless. Removing the unit dyadic (idemfactor) from the quadrupole yields the traceless tensor

$$\int s(\boldsymbol{r}')(\boldsymbol{r}'\boldsymbol{r}')\,\mathrm{d}^3r' \Rightarrow \int s(\boldsymbol{r}')\left(\boldsymbol{r}'\boldsymbol{r}' - \tfrac{1}{3}\,r'^2\,\boldsymbol{I}\right)\mathrm{d}^3r' \tag{20}$$

The differences between various scalar multipole expansions and the relationship between their multipole moments are discussed in more detail by Geselowitz (1965) and Wikswo and Swinney (1984).

2.4. Generalization of the Taylor series multipole expansion

The scalar multipole expansions presented in section 2.1 (spherical coordinates) and section 2.2 (Cartesian coordinates) are based on a series expansion of the scalar Green's function in (4). These expansions are therefore only useful if we wish to expand a field that can be written in the form given in (2). As this is not always the case and since it is useful to be able to readily expand fields produced by a vector source $\boldsymbol{s}(\boldsymbol{r}')$, we now generalize the use of a Taylor series to obtain a multipole expansion of any field $\psi(\boldsymbol{r})$ given by

$$\psi(\boldsymbol{r}) = \frac{1}{4\pi}\int \boldsymbol{s}(\boldsymbol{r}')\cdot\Phi(\boldsymbol{r}, \boldsymbol{r}')\,\mathrm{d}^3r'. \tag{21}$$

The Taylor expansion of $\Phi(\boldsymbol{r}, \boldsymbol{r}')$ about an arbitrary location $\boldsymbol{l}$ is given by

$$\Phi(\boldsymbol{r}, \boldsymbol{r}') = \sum_{n=0}^{\infty}\frac{1}{n!}[(\boldsymbol{r}' - \boldsymbol{l})\cdot\nabla_l]^n\Phi(\boldsymbol{r}, \boldsymbol{l}) \tag{22}$$

where ∇_l is defined as

$$\nabla_l\phi(\boldsymbol{r}, \boldsymbol{l}) \equiv \nabla'(\phi(\boldsymbol{r}, \boldsymbol{r}')|_{\boldsymbol{r}'=\boldsymbol{l}}. \tag{23}$$

Inserting (22) in (21) and borrowing the notation used by Castellanos *et al* (1978) yields

$$\psi(\boldsymbol{r}) = \frac{1}{4\pi} \sum_{n=0}^{\infty} \frac{1}{n!} \int \boldsymbol{s}(\boldsymbol{r}')[(\boldsymbol{r}' - \boldsymbol{l}) \cdot \nabla_l]^n \Phi(\boldsymbol{r}, \boldsymbol{l}) \, \mathrm{d}^3 r' \tag{24}$$

$$= \frac{1}{4\pi} \sum_{n=0}^{\infty} \nabla_l^n \Phi(\boldsymbol{r}, \boldsymbol{l}) \parallel \Omega^n \tag{25}$$

where the double vertical bars denote the n-fold contractions between the two polyads ∇_l^n (the nth consecutive derivative w.r.t. to $\boldsymbol{l}$) and Ω^n (the nth order moments) is defined by

$$\Omega^n = \frac{1}{n!} \int (\boldsymbol{r}' - \boldsymbol{l})^n \boldsymbol{s}(\boldsymbol{r}') \, \mathrm{d}^3 r'. \tag{26}$$

For instance, a first-order approximation of the scalar field defined by (21) is thus given by dipolar and quadrupolar terms and can be explicitly computed using (25) and (26) to yield

$$\psi(\boldsymbol{r}) \simeq \frac{1}{4\pi} \left(\int \boldsymbol{s}(\boldsymbol{r}') \, \mathrm{d}^3 r' \cdot \boldsymbol{\Phi}(\boldsymbol{r}, \boldsymbol{l}) + \int (\boldsymbol{r}' - \boldsymbol{l}) \boldsymbol{s}(\boldsymbol{r}') \, \mathrm{d}^3 r' : \nabla_l \boldsymbol{\Phi}(\boldsymbol{r}, \boldsymbol{l}) \right). \tag{27}$$

3. Current multipole expansion in Cartesian coordinates

3.1. Introduction

Magnetoencephalographic measurements arise from quasi-static bioelectric source currents inside the head. Under the quasi-static approximation, the *vector potential* satisfies Poisson's equation $\nabla^2 \boldsymbol{A}(\boldsymbol{r}) = -\mu_0 \boldsymbol{J}(\boldsymbol{r})$. Thus the solution for a localized source distribution is

$$\boldsymbol{A}(\boldsymbol{r}) = \frac{\mu_0}{4\pi} \int \frac{\boldsymbol{J}(\boldsymbol{r}')}{|\boldsymbol{r} - \boldsymbol{r}'|} \, \mathrm{d}^3 r' \tag{28}$$

where volume integral is over the region of non-zero current density $\boldsymbol{J}(\boldsymbol{r}')$. The *magnetic induction* $\boldsymbol{B}(\boldsymbol{r})$ can be derived from $\boldsymbol{A}(\boldsymbol{r})$ as $\boldsymbol{B}(\boldsymbol{r}) = \nabla \times \boldsymbol{A}(\boldsymbol{r})$. Throughout this paper, we will assume the current density is well behaved and localized to a finite region, such that an enclosing surface may be formed just outside this region. Under this assumption, the standard vector identities readily convert the curl into the well-known law

$$\boldsymbol{B}(\boldsymbol{r}) = \frac{\mu_0}{4\pi} \int \boldsymbol{J}(\boldsymbol{r}') \times \frac{(\boldsymbol{r} - \boldsymbol{r}')}{|\boldsymbol{r} - \boldsymbol{r}'|^3} \, \mathrm{d}^3 r'. \tag{29}$$

If we observe just the radial component of this field, the solution further simplifies to

$$\frac{\boldsymbol{r}}{r} \cdot \boldsymbol{B}(\boldsymbol{r}) = \frac{\mu_0}{4\pi} \int \frac{\boldsymbol{r} \cdot \boldsymbol{r}' \times \boldsymbol{J}(\boldsymbol{r}')}{r|\boldsymbol{r} - \boldsymbol{r}'|^3} \, \mathrm{d}^3 r'. \tag{30}$$

An important and widely used substitution in MEG is to partition the current density into a *primary current density* $\boldsymbol{J}^p(\boldsymbol{r}')$ and a *volume current* $\boldsymbol{J}^v(\boldsymbol{r}')$. The volume currents flow in response to the local variations in the potential, $\boldsymbol{J}^v(\boldsymbol{r}') = -\sigma(\boldsymbol{r}')\nabla' V(\boldsymbol{r}')$, where $\sigma(\boldsymbol{r}')$ is the conductivity, which we assume to be isotropic. The more important primary currents are the 'generators' of these volume currents. In other words, neural activity generates primary currents in specific regions of the brain that then flow passively throughout the entire brain to complete the 'circuit'.

A further important assumption is to assume that regions of conductivity are homogeneous, with known boundaries enclosing these surfaces. Given a piecewise homogeneous volume

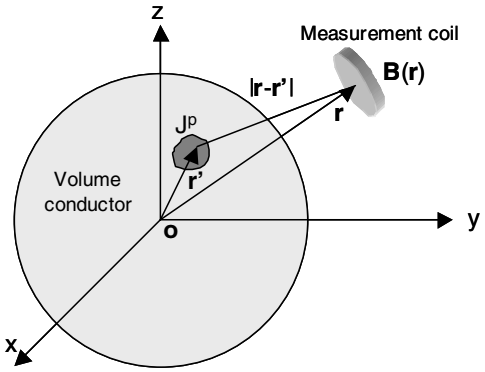

Figure 2. *MEG primary model*: radial MEG sensors measure the external magnetic field caused by a localized neural source distribution $\boldsymbol{J}^p$ within a spherically symmetric conducting head model.

conductor, the total current density $\boldsymbol{J}(\boldsymbol{r}')$ in (28) satisfies (Geselowitz 1970, Grynszpan and Geselowitz 1973)

$$\boldsymbol{J}(\boldsymbol{r}')\,\mathrm{d}^3r' = \boldsymbol{J}^p(\boldsymbol{r}')\,\mathrm{d}^3r' - \sum_{ij}(\sigma_i - \sigma_j)V(\boldsymbol{r}')\,\mathrm{d}\boldsymbol{S}'_{ij} \tag{31}$$

where the vector element of surface $\mathrm{d}\boldsymbol{S}'_{ij}$ is directed from the ith region to the jth region and V is the electric potential on this surface. Accordingly, the vector potential $\boldsymbol{A}$ can be split into a primary and a secondary component $\boldsymbol{A} = \boldsymbol{A}^p + \boldsymbol{A}^v$,

$$\boldsymbol{A}^p(\boldsymbol{r}) = \frac{\mu_0}{4\pi}\int \frac{\boldsymbol{J}^p(\boldsymbol{r}')}{|\boldsymbol{r}-\boldsymbol{r}'|}\,\mathrm{d}^3r' \tag{32}$$

$$\boldsymbol{A}^v(\boldsymbol{r}) = -\frac{\mu_0}{4\pi}\sum_{ij}(\sigma_i - \sigma_j)\int_{S_{ij}} \frac{V(\boldsymbol{r}')}{|\boldsymbol{r}-\boldsymbol{r}'|}\,\mathrm{d}\boldsymbol{S}'_{ij}. \tag{33}$$

Thus the primary and volume field contributions can be expressed respectively as

$$\boldsymbol{B}^p(\boldsymbol{r}) = \frac{\mu_0}{4\pi}\int \boldsymbol{J}^p(\boldsymbol{r}') \times \frac{(\boldsymbol{r}-\boldsymbol{r}')}{|\boldsymbol{r}-\boldsymbol{r}'|^3}\,\mathrm{d}^3r', \tag{34}$$

$$\boldsymbol{B}^v(\boldsymbol{r}) = \frac{\mu_0}{4\pi}\sum_{ij}(\sigma_i - \sigma_j)\int_{S_{ij}} V(\boldsymbol{r}')\frac{(\boldsymbol{r}-\boldsymbol{r}')}{|\boldsymbol{r}-\boldsymbol{r}'|^3} \times \mathrm{d}\boldsymbol{S}'_{ij}. \tag{35}$$

If the volume conductor comprises spherically symmetric regions of homogeneous conductivity, then all surfaces in (31) are radial, and substitution of (31) into (30) reveals that the contribution from the volume currents vanishes. In other words, the volume currents $\boldsymbol{J}^v$ do not contribute to the radial component of the magnetic field outside a spherically symmetric volume conductor. This result applies also, in the limiting case, to the component normal to a homogeneous conducting half-space. Radial measurements outside a spherically symmetric conductor and normal measurements outside a homogeneous half-space are the most basic models used in MEG and MCG respectively. In both cases the CME can be derived without taking the volume current into consideration. In this section we use the term *primary model* when referring to a spherically symmetric conductor and a radial sensor configuration (figure 2). Expanding the field outside such a model yields an expansion of the radial field B_r which we refer to as a *primary CME*. In contrast, a *full CME* denotes an expansion of the full magnetic field $\boldsymbol{B}$ outside an arbitrary volume conductor.

3.2. Primary CME about an arbitrary expansion point

Typically, a Cartesian expansion of the primary magnetic field is achieved by first expanding the vector potential and then taking the curl of the result. Although this is not the only possible method, it is straightforward and has been widely used in MCG source localization (e.g. Katila 1983, Nenonen *et al* 1991).

In most of the available literature, especially within the MCG community, multipole expansions are presented as expansions about the origin of the coordinate system. Since it is advantageous to expand the field about the centroid of the source, which is not necessarily at the origin of a fixed coordinate system, some authors (e.g. Nolte and Curio 1997) use a coordinate system with a variable origin. Here, we will explicitly derive the equations for the general case of a multipole expansion about an arbitrary location $\boldsymbol{l}$ for a fixed coordinate system.

The vector potential due to the primary current given in (32) follows the form of (19). Inserting the first two terms of the Taylor expansion of the Green's function given in (12) in the expression for the vector potential in (32) yields

$$\boldsymbol{A}^p(\boldsymbol{r}) = \frac{\mu_0}{4\pi}\frac{1}{|\boldsymbol{r}-\boldsymbol{l}|}\int_{v'}\boldsymbol{J}^p(\boldsymbol{r}')\,\mathrm{d}^3r' + \frac{\mu_0}{4\pi}\frac{\boldsymbol{r}-\boldsymbol{l}}{|\boldsymbol{r}-\boldsymbol{l}|^3}\cdot\int_{v'}(\boldsymbol{r}'-\boldsymbol{l})\boldsymbol{J}^p(\boldsymbol{r}')\,\mathrm{d}^3r' + \cdots . \tag{36}$$

The two integrals in (36) represent the first two source moments of the expansion

$$\boldsymbol{q} = \int_{v'}\boldsymbol{J}^p(\boldsymbol{r}')\,\mathrm{d}^3r' \tag{37}$$

$$\tilde{\boldsymbol{Q}}_E = \int_{v'}(\boldsymbol{r}'-\boldsymbol{l})\,\boldsymbol{J}^p(\boldsymbol{r}')\,\mathrm{d}^3r' \tag{38}$$

where $\boldsymbol{q}$ is the current dipole and $\tilde{\boldsymbol{Q}}_E$ is a 'locally defined' current quadrupole. The expansion in (36) can be written as

$$\boldsymbol{A}^p(\boldsymbol{r}) = \frac{\mu_0}{4\pi}\frac{\boldsymbol{q}}{|\boldsymbol{r}-\boldsymbol{l}|} + \frac{\mu_0}{4\pi}\frac{\boldsymbol{r}-\boldsymbol{l}}{|\boldsymbol{r}-\boldsymbol{l}|^3}\cdot\tilde{\boldsymbol{Q}}_E + \cdots . \tag{39}$$

We use the notation $\tilde{\boldsymbol{Q}}_E$ to distinguish between multipole moment for expansions defined about an arbitrary location and those defined about the origin of the coordinate system. The quadrupole moments of the latter are $\boldsymbol{Q}_E = \int_{v'}\boldsymbol{r}'\boldsymbol{J}^p(\boldsymbol{r}')\,\mathrm{d}^3r'$. It is easy to see that $\tilde{\boldsymbol{Q}}_E$ and $\boldsymbol{Q}_E$ are related by

$$\tilde{\boldsymbol{Q}}_E = \boldsymbol{Q}_E - \boldsymbol{l}\boldsymbol{q}. \tag{40}$$

An important property of multipole expansions is that the first non-vanishing moment is independent of the expansion origin $\boldsymbol{l}$ whereas higher moments are not. The first non-vanishing moment in the expansion of the vector potential in (39) is the current dipole $\boldsymbol{q}$, which is origin independent. The current quadrupole $\tilde{\boldsymbol{Q}}_E$ clearly depends on the expansion point $\boldsymbol{l}$. This dependency is directly related to the shift theorem formulated by Geselowitz (1965) which describes the relationships between multipole representations as a function of the expansion point. In the particular case where the monopole term is zero, the dipole components remain the same while the quadrupole components can be computed using shift equations. These equations express the new quadrupole moments in terms of the dipole and quadrupole moments of the original expansion. The shift equations through the octupolar moments for the spherical harmonic multipole expansion are given by Wikswo and Swinney (1985).

Applying the curl operator to A^p in (39) yields

$$\boldsymbol{B}^p(\boldsymbol{r}) = \nabla\times\boldsymbol{A}^p(\boldsymbol{r}) = \frac{\mu_0}{4\pi}\nabla\times\left(\frac{\boldsymbol{q}}{|\boldsymbol{r}-\boldsymbol{l}|}\right) + \frac{\mu_0}{4\pi}\nabla\times\left(\frac{\boldsymbol{r}-\boldsymbol{l}}{|\boldsymbol{r}-\boldsymbol{l}|^3}\cdot\tilde{\boldsymbol{Q}}_E\right) + \cdots . \tag{41}$$

After considerable manipulations (appendix A) we obtain the expansion

$$\boldsymbol{B}^p(\boldsymbol{r}) = \frac{\mu_0}{4\pi}\frac{\boldsymbol{q}\times\boldsymbol{r}}{|\boldsymbol{r}-\boldsymbol{l}|^3} + \frac{\mu_0}{4\pi}\frac{2\,\boldsymbol{m}^p}{|\boldsymbol{r}-\boldsymbol{l}|^3} + \frac{\mu_0}{4\pi}\frac{3\,((\boldsymbol{r}-\boldsymbol{l})\cdot\tilde{\boldsymbol{Q}}_E)\times(\boldsymbol{r}-\boldsymbol{l})}{|\boldsymbol{r}-\boldsymbol{l}|^5} + \cdots \tag{42}$$

where $\boldsymbol{m}_p$ is the *primary* magnetic dipole moment, i.e. defined in terms of the primary current density only, and given by

$$\boldsymbol{m}^p = \frac{1}{2}\int_{v'} \boldsymbol{r}'\times\boldsymbol{J}^p(\boldsymbol{r}')\,\mathrm{d}^3r'. \tag{43}$$

Using (42) and $B_r(\boldsymbol{r}) = \boldsymbol{B}^p(\boldsymbol{r})\cdot\boldsymbol{e}_r$ the multipole expansion of the radial component of the magnetic field about a location $\boldsymbol{l}$ outside a spherically symmetric conductor is given by

$$B_r(\boldsymbol{r}) = \frac{\mu_0}{4\pi}\frac{\boldsymbol{r}}{|r|}\cdot\left(\frac{2\boldsymbol{m}^p}{|\boldsymbol{r}-\boldsymbol{l}|^3} - \frac{3\,((\boldsymbol{r}-\boldsymbol{l})\cdot\tilde{\boldsymbol{Q}}_E))\times\boldsymbol{l}}{|\boldsymbol{r}-\boldsymbol{l}|^5} + \cdots\right) \tag{44}$$

or alternatively using the dyadic contraction notation we can write

$$B_r(\boldsymbol{r}) = \frac{\mu_0}{4\pi r}\left(\frac{2\boldsymbol{m}^p\cdot\boldsymbol{r}}{|\boldsymbol{r}-\boldsymbol{l}|^3} + \frac{3(\boldsymbol{r}\times\boldsymbol{l})(\boldsymbol{r}-\boldsymbol{l})}{|\boldsymbol{r}-\boldsymbol{l}|^5} : \tilde{\boldsymbol{Q}}_E + \cdots\right). \tag{45}$$

The expansion form in (45) is given as a sum of a primary magnetic dipole $\boldsymbol{m}^p$ and a current quadrupole $\tilde{\boldsymbol{Q}}_E = \boldsymbol{Q}_E - \boldsymbol{l}\boldsymbol{q}$. For consistency and simplicity, we would also like to reformulate this initial expansion in terms of just a current dipole and a current quadrupole. We achieve this substitution by introducing the cross product tensor $\boldsymbol{X}_r$ defined by $\boldsymbol{r}\times\boldsymbol{x} \equiv \boldsymbol{X}_r\cdot\boldsymbol{x}$. Now using the relationship $\boldsymbol{X}_r : \tilde{\boldsymbol{Q}}_E = 2\,\boldsymbol{r}\cdot\boldsymbol{m}^p - \boldsymbol{r}\times\boldsymbol{l}\cdot\boldsymbol{q}$ we can rewrite (45) as

$$B_r(\boldsymbol{r}) = \frac{\mu_0}{4\pi r}\left(\frac{\boldsymbol{r}\times\boldsymbol{l}\cdot\boldsymbol{q}}{|\boldsymbol{r}-\boldsymbol{l}|^3} + \frac{3\,(\boldsymbol{r}\times\boldsymbol{l})(\boldsymbol{r}-\boldsymbol{l}) + |\boldsymbol{r}-\boldsymbol{l}|^2\boldsymbol{X}_r}{|\boldsymbol{r}-\boldsymbol{l}|^5} : \tilde{\boldsymbol{Q}}_E + \cdots\right). \tag{46}$$

Truncating the expansion in (46) after the quadrupolar term gives a first-order approximation of the radial field outside a spherically symmetric conductor which can be written as

$$B_r(\boldsymbol{r}) = \frac{\mu_0}{4\pi}\boldsymbol{k}_D\cdot\boldsymbol{q} + \frac{\mu_0}{4\pi}\boldsymbol{k}_Q : \tilde{\boldsymbol{Q}}_E. \tag{47}$$

where the dipole gain vector $\boldsymbol{k}_D$ and the 3×3 quadrupole gain tensor $\boldsymbol{k}_Q$ are defined by

$$\boldsymbol{k}_D(\boldsymbol{r},\boldsymbol{l}) \equiv \frac{\boldsymbol{r}\times\boldsymbol{l}}{r\,|\boldsymbol{r}-\boldsymbol{l}|^3} \tag{48}$$

$$\boldsymbol{k}_Q(\boldsymbol{r},\boldsymbol{l}) \equiv \frac{3\,(\boldsymbol{r}\times\boldsymbol{l})(\boldsymbol{r}-\boldsymbol{l}) + |\boldsymbol{r}-\boldsymbol{l}|^2\,\boldsymbol{X}_r}{r\,|\boldsymbol{r}-\boldsymbol{l}|^5}. \tag{49}$$

We can easily verify that the terms $\boldsymbol{k}_D$ and $\boldsymbol{k}_\mathrm{Q}$ are related by

$$\boldsymbol{k}_Q(\boldsymbol{r},\boldsymbol{l}) = \nabla_l\,\boldsymbol{k}_D(\boldsymbol{r},\boldsymbol{l}) \tag{50}$$

where ∇_l is the gradient defined in (23). This result is in agreement with the general expansion given in (27).

3.3. Primary CME about the origin of the coordinate system

The multipole expansion about the origin of the coordinate system is immediately obtained by inserting $\boldsymbol{l} = \boldsymbol{0}$ in (42)

$$\boldsymbol{B}^p(\boldsymbol{r}) \simeq \frac{\mu_0}{4\pi}\left(\frac{\boldsymbol{q}\times\boldsymbol{r}}{r^3} + \frac{2\boldsymbol{m}^p}{r^3} + \frac{3\,(\boldsymbol{r}\cdot\boldsymbol{Q}_E)\times\boldsymbol{r}}{r^5}\right). \tag{51}$$

Equation (51) and the relationship $B_r(\boldsymbol{r}) = \boldsymbol{B}^p(\boldsymbol{r}) \cdot \boldsymbol{e}_r$ give the first-order *current* multipole expansion of the radial magnetic field about the origin for a spherically symmetric conductor

$$B_r(\boldsymbol{r}) \simeq \frac{\mu_0}{4\pi} \frac{2\,\boldsymbol{m}^p \cdot \boldsymbol{r}}{r^4}. \tag{52}$$

The contributions of the first and third term in (51) vanish. This result is easily verified by computing the radial component of the magnetic field as defined by Jackson (1975, p 182) assuming a spherically symmetric conductor. Finally, (51) can also be used to obtain the z-component of the magnetic field $B_z = \boldsymbol{B} \cdot \boldsymbol{e}_z$, yielding the same expression for B_z used in Katila and Karp (1983). One noteworthy observation is that B_z contains explicit contributions from the current dipole, the primary magnetic dipole and symmetric quadrupole terms whereas B_r, as defined in (52), only shows the contribution of a magnetic dipole. This difference is important when attempting to relate multipole expansions for primary sources in MCG to the expansions needed in MEG.

From the three source terms in (51) we distinctly see the separate contribution of a current dipole $\boldsymbol{q}$, a magnetic dipole $\boldsymbol{m}^p$ and a current quadrupole term $\boldsymbol{Q}_E$ to the magnetic field. These separations imply that both electric and magnetic moments contribute to the magnetic field measured outside the localized source. Indeed, it has been shown (Grynszpan and Geselowitz 1973, Haberkorn 1994, Nolte and Curio 1997) that while this is the case for the expansion of the magnetic field, it is not true for the *electric* scalar potential V. Performing the multipole expansion of the latter shows that only the electric multipoles contribute to the external electric potential.

An equivalent statement is made by Katila and Karp (1983) and Wikswo (1983) by identifying the electric and magnetic coefficients in the quadrupole tensor $\boldsymbol{Q}_E$. By writing the quadrupole tensor as a sum of its symmetric and anti-symmetric parts, the authors show that the magnetic dipole moment is given by the anti-symmetric part of the tensor and that it is electrically silent (these moments represent current loops). Only the symmetric portion of the quadrupole tensor contributes to the electric potential measurements. In other words, electric potential measurements give no information about magnetic dipole moments. These can only be obtained through magnetic measurements.

3.4. Full CME about an arbitrary expansion point

The above expansions of the primary current do not directly address the volume currents that contribute to other components of the external magnetic field. Direct extensions of the expansions to the volume currents in terms of expansions of the vector potential involve complex manipulations based on vector spherical harmonics (Grynszpan and Geselowitz 1973, Jackson 1975). In the next section, we will develop an alternative approach to expanding these currents by considering instead the magnetic scalar potential. A result of that development used in this section is the integral expression for the magnetic scalar potential caused by a localized current density $\boldsymbol{J}$, stated as (Bronzan 1971),

$$V_m(\boldsymbol{r}) = \frac{1}{4\pi} \int \frac{\boldsymbol{J}(\boldsymbol{r}') \cdot \boldsymbol{r} \times \boldsymbol{r}'}{|\boldsymbol{r} - \boldsymbol{r}'|[r|\boldsymbol{r} - \boldsymbol{r}'| + r^2 - \boldsymbol{r} \cdot \boldsymbol{r}']}\, \mathrm{d}^3 r'. \tag{53}$$

As noted by Bronzan (1971), (53) is valid for an arbitrary coordinate system and a localized source, where the observation point $\boldsymbol{r}$ is outside the source and does not lie on a line between the origin and the source. Therefore, if we place the origin inside the source body, these equations hold for all points outside of the body. Furthermore, if the body is spherically homogeneous about the origin, then direct insertion of (31) into the numerator of (53) easily

reveals that the formula simplifies by replacing $\boldsymbol{J}(\boldsymbol{r}')$ by $\boldsymbol{J}^p(\boldsymbol{r}')$. Therefore, the magnetic potential outside a spherically symmetric volume conductor is given by

$$V_m(\boldsymbol{r}) = \frac{1}{4\pi} \int \left(\frac{\boldsymbol{r} \times \boldsymbol{r}'}{F(\boldsymbol{r}, \boldsymbol{r}')} \right) \cdot \boldsymbol{J}^p(\boldsymbol{r}') \, \mathrm{d}^3 r' \tag{54}$$

where we define the function F to represent the denominator in (53), $F(\boldsymbol{r}, \boldsymbol{r}') = |\boldsymbol{r} - \boldsymbol{r}'|(r\,|\boldsymbol{r} - \boldsymbol{r}'| + r^2 - \boldsymbol{r}' \cdot \boldsymbol{r})$.

As this model is so widely used in MEG, we elaborate on its CME development here. Comparing (54) with the general form in (21) yields the identities $\psi(\boldsymbol{r}) = V_m(\boldsymbol{r})$, $\boldsymbol{s}(\boldsymbol{r}') = \boldsymbol{J}^p(\boldsymbol{r}')$, and $\Phi(\boldsymbol{r}, \boldsymbol{r}') = -(\boldsymbol{r} \times \boldsymbol{r}'/F(\boldsymbol{r}, \boldsymbol{r}'))$. Consequently, (25) yields

$$V_m(\boldsymbol{r}) = \frac{1}{4\pi} \sum_{n=0}^{\infty} \nabla_l^n \left(\frac{\boldsymbol{r} \times \boldsymbol{l}}{F(\boldsymbol{r}, \boldsymbol{l})} \right) \| \Omega^n \tag{55}$$

where the nth order current moments are defined in (26) yielding

$$\Omega^n = \frac{1}{n!} \int (\boldsymbol{r}' - \boldsymbol{l})^n \, \boldsymbol{J}^p(\boldsymbol{r}') \, \mathrm{d}\boldsymbol{r}'. \tag{56}$$

Since the magnetic field satisfies $\boldsymbol{B}(\boldsymbol{r}) = -\mu_0 \nabla V_m(\boldsymbol{r})$, we can write the full CME of $\boldsymbol{B}(\boldsymbol{r})$ up to the nth order as

$$\begin{aligned} \boldsymbol{B}(\boldsymbol{r}) &= -\frac{\mu_0}{4\pi} \sum_{n=0}^{\infty} \nabla_l^n \left[\nabla \left(\frac{\boldsymbol{r} \times \boldsymbol{l}}{F(\boldsymbol{r}, \boldsymbol{l})} \right) \right] \| \Omega^n \\ &= -\frac{\mu_0}{4\pi} \sum_{n=0}^{\infty} \nabla_l^n \left[\frac{F \, \boldsymbol{X}_l + \nabla F \, (\boldsymbol{l} \times \boldsymbol{r})}{F^2} \right] \| \Omega^n \end{aligned} \tag{57}$$

where $F = F(\boldsymbol{r}, \boldsymbol{l})$. We may now rewrite the infinite CME about an arbitrary location $\boldsymbol{l}$ as

$$\boldsymbol{B}(\boldsymbol{r}) = \sum_{n=0}^{\infty} \boldsymbol{B}^n(\boldsymbol{r}, \boldsymbol{l}) \tag{58}$$

such that the magnetic field of the nth order current multipole located at $\boldsymbol{l}$ is defined by

$$\boldsymbol{B}^n(\boldsymbol{r}, \boldsymbol{l}) = -\frac{\mu_0}{4\pi} \nabla_l^n \left[\frac{F \boldsymbol{X}_l + \nabla F \, (\boldsymbol{l} \times \boldsymbol{r})}{F^2} \right] \| \Omega^n. \tag{59}$$

The zeroth-order ($n = 0$) is the dipole field,

$$\boldsymbol{B}^0(\boldsymbol{r}, \boldsymbol{l}) = \boldsymbol{B}_{\mathrm{dip}}(\boldsymbol{r}, \boldsymbol{l}) = \boldsymbol{G}_{\mathrm{dip}}(\boldsymbol{r}, \boldsymbol{l}) \cdot \boldsymbol{q} \tag{60}$$

where we define the dipole gain vector as

$$\boldsymbol{G}_{\mathrm{dip}}(\boldsymbol{r}, \boldsymbol{l}) = -\frac{\mu_0}{4\pi} \left[\frac{F \boldsymbol{X}_l + \nabla F \, (\boldsymbol{l} \times \boldsymbol{r})}{F^2} \right] \tag{61}$$

and the current dipole moment is $\boldsymbol{q} = \Omega^0 = \int \boldsymbol{J}^p(\boldsymbol{r}') \, \mathrm{d}\boldsymbol{r}'$. Inserting (61) in (59) enables us to write the gain polyad of the nth order current multipole as

$$\boldsymbol{B}^n(\boldsymbol{r}, \boldsymbol{l}) = \nabla_l^n (\boldsymbol{G}_{\mathrm{dip}}(\boldsymbol{r}, \boldsymbol{l})) \| \Omega^n. \tag{62}$$

Equation (62) shows that all nth order-multipole fields can be computed in terms of the nth-order derivatives of the dipole gain $\boldsymbol{G}_{\mathrm{dip}}$ with respect to the dipole location, in agreement with the general statement in Nolte and Curio (1997).

Finally, the full CME about an arbitrary expansion point $\boldsymbol{l}$ is obtained by inserting (62) in (58) yielding

$$\boldsymbol{B}(\boldsymbol{r}) = \sum_{n=0}^{\infty} \nabla_l^n (\boldsymbol{G}_{\mathrm{dip}}(\boldsymbol{r}, \boldsymbol{l})) \| \Omega^n \tag{63}$$

where the current multipole moments Ω^n are given in (56) and the dipole gain is given in (61).

As a result, the first-order approximation of the CME of the full magnetic field outside a spherically symmetric volume conductor is

$$\boldsymbol{B}(\boldsymbol{r}) = -\frac{\mu_0}{4\pi}\left[\frac{F\boldsymbol{X}_l + \nabla F(\boldsymbol{l}\times\boldsymbol{r})}{F^2}\right]\cdot\boldsymbol{q} \;-\; \frac{\mu_0}{4\pi}\nabla_l\left(\frac{F\boldsymbol{X}_l + \nabla F(\boldsymbol{l}\times\boldsymbol{r})}{F^2}\right):\tilde{\boldsymbol{Q}}_E + \cdots \tag{64}$$

where the moments $\boldsymbol{q}$ and $\tilde{\boldsymbol{Q}}_E$ are defined in (37) and (38) respectively.

The first term in (64) can be written as

$$\boldsymbol{B}_{\text{dip}}(\boldsymbol{r}) = \frac{\mu_0}{4\pi}\,\frac{F\boldsymbol{q}\times\boldsymbol{l} - (\boldsymbol{q}\times\boldsymbol{l}\cdot\boldsymbol{r})\,\nabla F}{F^2} \tag{65}$$

which is the well-known equation (Sarvas 1987) for the magnetic field outside a spherical head model, given a current dipole of moment $\boldsymbol{q}$ at location $\boldsymbol{l}$. The second term in (64) is the quadrupolar field and has not been explicitly expanded for brevity (see Mosher *et al* 2000 for explicit expansions of the gradients).

The equations for the first-order primary and full CME about an arbitrary expansion point given a spherically symmetric volume conductor are summarized in table 1. A comparable development of this expansion may be found in Nolte and Curio (1997).

Table 1. The first-order current multipole expansion (CME) about an arbitrary point $\boldsymbol{l}$ of the radial and full magnetic fields outside a spherically symmetric conductor. Higher order terms (octupole, hexadecapole, etc) for the full CME can be directly deduced from equation (62).

Full expansion	$\boldsymbol{B}(\boldsymbol{r}) = -\frac{\mu_0}{4\pi}\left[\frac{F\boldsymbol{X}_l + \nabla F(\boldsymbol{l}\times\boldsymbol{r})}{F^2}\right]\cdot\boldsymbol{q} - \frac{\mu_0}{4\pi}\nabla_l\left(\frac{F\boldsymbol{X}_l + \nabla F(\boldsymbol{l}\times\boldsymbol{r})}{F^2}\right):\tilde{\boldsymbol{Q}}_E + \cdots$
Radial expansion	$B_r(\boldsymbol{r}) = \frac{\mu_0}{4\pi}\frac{\boldsymbol{r}\times\boldsymbol{l}}{r\,\lvert\boldsymbol{r}-\boldsymbol{l}\rvert^3}\cdot\boldsymbol{q} + \frac{\mu_0}{4\pi}\frac{3\,(\boldsymbol{r}\times\boldsymbol{l})(\boldsymbol{r}-\boldsymbol{l}) + \lvert\boldsymbol{r}-\boldsymbol{l}\rvert^2\boldsymbol{X}_r}{r\lvert\boldsymbol{r}-\boldsymbol{l}\rvert^5} : \tilde{\boldsymbol{Q}}_E + \cdots$
Moments	$\boldsymbol{q} = \int_{v'}\boldsymbol{J}^p(\boldsymbol{r}')\,\mathrm{d}^3r' \quad\text{and}\quad \tilde{\boldsymbol{Q}}_E = \int_{v'}(\boldsymbol{r}'-\boldsymbol{l})\,\boldsymbol{J}^p(\boldsymbol{r}')\,\mathrm{d}^3r'$

4. Magnetic multipole expansion in spherical coordinates

4.1. Background

We now consider a *magnetic multipole expansion* (MME) framework with magnetic moments defined in terms of the effective *magnetic moment density* $\boldsymbol{r}'\times\boldsymbol{J}(\boldsymbol{r}')$. As in the previous section, if the volume conductor is spherically symmetric about the same origin, then the MMEs conveniently simplify to forms that only involve the primary current density.

In order to obtain an MME of the field measured outside the head using arbitrarily oriented MEG sensors, an expression for the multipole expansion of the complete magnetic field $\boldsymbol{B}$ is required. The inner product of the field with the true orientation of each sensor will then lead to the desired expansion of the scalar measurement field. Maxwell's equations for the quasi-static magnetic field are

$$\nabla\times\boldsymbol{B} = \mu_0\boldsymbol{J} \tag{66}$$

$$\nabla\cdot\boldsymbol{B} = 0 \tag{67}$$

where $\boldsymbol{J}$ denotes the total current density. In the region outside the current source, the magnetic field satisfies $\nabla\times\boldsymbol{B} = 0$, and can therefore be represented as a gradient of a magnetic scalar potential $V_m(\boldsymbol{r})$,

$$\boldsymbol{B} = -\mu_0\nabla V_m. \tag{68}$$

Hence we have

$$\boldsymbol{r} \cdot \boldsymbol{B} = -\mu_0 r \frac{\partial V_m}{\partial r} \tag{69}$$

or

$$B_r = -\mu_0 \frac{\partial V_m}{\partial r}. \tag{70}$$

Inserting (68) in (67) yields $\nabla^2 V_m = 0$. Thus V_m is harmonic and uniquely determined by its radial derivative and by the requirement that it vanish at infinity. We can therefore use the radial component of the field to determine the scalar magnetic potential using

$$V_m = \frac{1}{\mu_0} \int_{\xi=r}^{\infty} B_r(\xi \boldsymbol{e}_r)\, \mathrm{d}\xi \tag{71}$$

where $\boldsymbol{e}_r$ is the radial unit vector. Inserting the expression of the radial field B_r into (71) leads to an integral over ξ. The complete magnetic field $\boldsymbol{B}$ is then obtained using (68).

This method was first presented by Bronzan (1971) and a similar approach was given by Gray (1978). In both papers the aim was to obtain a spherical harmonic expansion of the magnetic field using the scalar magnetic potential instead of the vector magnetic potential. This same procedure was independently used by Sarvas (1987) in order to derive the closed form expression (65) for the full magnetic field produced by the current dipole in a spherically symmetric conductor.

The above equations are in accordance with a general theorem stating that at a source-free field point the complete magnetic field $\boldsymbol{B}(\boldsymbol{r})$ can be determined by its radial component. The theorem has been proved rigorously by Bouwkamp and Casimir (1954). A brief plausibility argument of the theorem is also given in the appendix of Gray (1978). An important consequence of (71) is that if the conductor is assumed to be spherically symmetric it is possible to compute the complete magnetic field $\boldsymbol{B}$ without knowledge of the conductivity profile, as we introduced in the previous section.

Deriving a multipole expansion of the complete magnetic field via the vector potential has been described for the general case of an inhomogeneous conductor by Grynszpan and Geselowitz (1973). The authors expanded the vector potential $\boldsymbol{A}$ via the expansion of the dyadic Green's function in terms of the solution functions of the vector Laplace equation in spherical coordinates (Morse 1953, pp 1799–1803). Bronzan (1971), however, noted that the awkward manipulations of the dyadic expansions can be avoided by using the expansion of the magnetic scalar potential $\boldsymbol{B} = -\mu_0 \nabla V_m$. We review his simpler development and the improvements by others.

4.2. Arbitrary volume conductor

Bronzan (1971) has shown that the complete multipole expansion of the magnetostatic field $\boldsymbol{B}$ outside a localized current density distribution $\boldsymbol{J}$ can be obtained using a procedure we refer to as the magnetic scalar potential method. His derivation consists of carrying out a line integral for V_m over the radial component of the magnetic field. The scalar magnetic potential outside a localized current distribution is hence

$$V_m(\boldsymbol{r}) = \frac{1}{\mu_0} \int_r^{\infty} \boldsymbol{B}(\xi \boldsymbol{e}_r) \cdot \boldsymbol{e}_r \, \mathrm{d}\xi \tag{72}$$

where $\boldsymbol{e}_r = \boldsymbol{r}/r$. Using (29), (72) can be written as

$$V_m(\boldsymbol{r}) = \frac{1}{4\pi} \int_r^{\infty} \int_{v'} \frac{\boldsymbol{J}(\boldsymbol{r}') \times (\xi \boldsymbol{e}_r - \boldsymbol{r}')}{|\xi \boldsymbol{e}_r - \boldsymbol{r}'|^3} \cdot \boldsymbol{e}_r \, \mathrm{d}^3 r' \, \mathrm{d}\xi \tag{73}$$

$$= \frac{1}{4\pi} \int_{v'} \boldsymbol{J}(\boldsymbol{r}') \cdot (\boldsymbol{e}_r \times \boldsymbol{r}') \int_r^{\infty} \frac{\mathrm{d}\xi}{|\xi \boldsymbol{e}_r - \boldsymbol{r}'|^3} \, \mathrm{d}^3 r'. \tag{74}$$

Computing the integral over ξ yields equation (53), presented in section 3.4 and used to obtain a CME of the full magnetic field. Explicit representation of the nth term in (63) is difficult. The MME of the full-field B is formally easier to derive if we first expand V_m, then apply the gradient to obtain a full expansion of $\boldsymbol{B}$.

We begin by stating (73) in the form (Bronzan 1971)

$$V_m(\boldsymbol{r}) = -\frac{1}{4\pi}\int_{v'} \nabla' \cdot [\boldsymbol{r}' \times \boldsymbol{J}(\boldsymbol{r}')] \int_r^\infty \frac{\mathrm{d}\xi}{\xi|\xi \boldsymbol{e}_r - \boldsymbol{r}'|}\, \mathrm{d}^3 r'. \tag{75}$$

The term $|\xi \boldsymbol{e}_r - \boldsymbol{r}'|^{-1}$ in (75) is a Green's function, and $\boldsymbol{r}' \times \boldsymbol{J}(\boldsymbol{r}')$ is the magnetic moment density or *magnetization* (Jackson 1975). Thus the difference between the MME and the CME approaches of the previous section is the rearrangement of the source term to be in terms of magnetization, rather than current density. Green's function can thus be expanded in spherical coordinates using (8). Hence

$$V_m(\boldsymbol{r}) = -\sum_{l=0}^{\infty}\sum_{m=-l}^{l} \frac{\hat{Y}_{lm}(\theta,\phi)}{2l+1} \int_{v'} r'^l \hat{Y}^*_{lm}(\theta',\phi')\, \nabla' \cdot [\boldsymbol{r}' \times \boldsymbol{J}(\boldsymbol{r}')] \int_r^\infty \xi^{-(l+2)}\, \mathrm{d}\xi\, \mathrm{d}^3 r'. \tag{76}$$

The integral over ξ is $\int_r^\infty 1/(\xi^{l+2})\,\mathrm{d}\xi = -\int_{1/r}^0 t^l\,\mathrm{d}t = (r^{-(l+1)})/((l+1))$. Therefore, the multipole expansion of the scalar magnetic potential in spherical harmonics is (Bronzan 1971),

$$\begin{aligned} V_m(\boldsymbol{r}) &= \sum_{l=0}^{\infty}\sum_{m=-l}^{l} \frac{M_{lm}}{2l+1}\frac{\hat{Y}_{lm}(\theta,\phi)}{r^{l+1}} \\ M_{lm} &= -\int_{v'} r'^l \hat{Y}^*_{lm}(\theta',\phi')\, \frac{\nabla' \cdot [\boldsymbol{r}' \times \boldsymbol{J}(\boldsymbol{r}')]}{l+1}\, \mathrm{d}^3 r' \end{aligned} \tag{77}$$

where M_{lm} are the magnetic multipole moments (3 for the dipole ($l = 1$), 5 for the quadrupole ($l = 2$) etc). The same result as in (77) was presented by Gray (1978) using a slightly different derivation, proceeding directly from the Maxwell equations.

For the sake of direct comparison with the related equations throughout the literature, we note that if we choose to use the non-normalized form of the spherical harmonics $Y_{lm}(\theta,\phi) = P_l^m(\cos\theta)\, e^{\mathrm{i}m\phi}$ and positive summation indices[5], (77) becomes

$$V_m(\boldsymbol{r}) = \frac{1}{4\pi}\mathrm{Re}\sum_{l=1}^{\infty}\sum_{m=0}^{l} M_{lm}\frac{Y^*_{lm}(\theta,\phi)}{r^{l+1}} \tag{78}$$

$$M_{lm} = -\frac{\gamma_{l,m}}{l+1}\int_{v'} r'^l Y_{lm}(\theta',\phi')\, \nabla' \cdot (\boldsymbol{r}' \times \boldsymbol{J}(\boldsymbol{r}'))\, \mathrm{d}^3 r' \tag{79}$$

or also[6]

$$M_{lm} = \frac{\gamma_{l,m}}{l+1}\int_{v'} \nabla' \left[r'^l Y_{lm}(\theta',\phi')\right] \cdot (\boldsymbol{r}' \times \boldsymbol{J}(\boldsymbol{r}'))\, \mathrm{d}^3 r' \tag{80}$$

where

$$\gamma_{l,m} = (2 - \delta_{m,0})\,\frac{(l-m)!}{(l+m)!}. \tag{81}$$

[5] Switching to positive summation indices, i.e. $m = 0, \ldots, l$, is common practice and is straightforward to do given that $\hat{Y}_{l,-m}(\theta,\phi) = (-1)^m \hat{Y}^*_{lm}(\theta,\phi)$. Note that the moment no longer contains the conjugate form of the spherical harmonic and that the initial value of the index l is 1.

[6] The moments of the spherical harmonic multipole expansion are of the form $A_{lm} = \int s(\boldsymbol{r}') f(\boldsymbol{r}')\,\mathrm{d}^3 r'$. It is easy to prove that for sources that are the negative divergence of a vector field $\boldsymbol{S}$, i.e. $s = -\nabla \cdot \boldsymbol{S}$, the moments reduce to the simpler from $A_{lm} = -\int f(\boldsymbol{r}')\nabla' \cdot \boldsymbol{S}(\boldsymbol{r}')\,\mathrm{d}V' = \int \nabla' f(\boldsymbol{r}') \cdot \boldsymbol{S}(\boldsymbol{r}')\,\mathrm{d}V'$ (e.g. Wikswo 1985, p 4304).

Finally, the expansion of the complete magnetic field $\boldsymbol{B}$ outside an inhomogeneous volume conductor is obtained using $\boldsymbol{B} = -\mu_0 \nabla V_m$ with (78) yielding

$$\boldsymbol{B}(\boldsymbol{r}) = -\frac{\mu_0}{4\pi} \operatorname{Re} \sum_{l=1}^{\infty} \sum_{m=0}^{l} M_{lm} \nabla \left(\frac{Y_{lm}^*(\theta, \phi)}{r^{l+1}} \right). \tag{82}$$

This result is identical to the expansion derived by Grynszpan and Geselowitz (1973, p 913) but has the advantage that it is derived without developing the full machinery of vector spherical harmonics.

4.3. Piecewise homogeneous head models

The results above are valid for a bounded inhomogeneous conductor, where $\boldsymbol{J}$ denotes the total current density. In regions of homogeneous conductivity, as discussed in Section 3.1, we may substitute (31) for the current density. The general form of the magnetic multipole moments of the full magnetic field outside a bounded piecewise homogeneous conductor can be derived from (80), yielding (Grynszpan and Geselowitz, 1973)

$$M_{lm} = \frac{\gamma_{l,m}}{l+1} \int \nabla' \left[r'^l Y_{lm}(\theta', \phi') \right] \cdot \boldsymbol{r}' \times \left[\boldsymbol{J}^p(\boldsymbol{r}') \, \mathrm{d}^3 r' - \sum_{ij} (\sigma_i - \sigma_j) V(\boldsymbol{r}') \, \mathrm{d}\boldsymbol{S}'_{ij} \right]. \tag{83}$$

As further discussed in section 3.1, if these homogeneous regions are spherically symmetric about the origin, then the contributions from the radial surfaces vanishes. Consequently, the multipole moments M_{lm} are given by

$$M_{lm} = \alpha_{lm} + \mathrm{i}\, \beta_{lm} = \frac{\gamma_{l,m}}{l+1} \int_{v'} \nabla' \left[r'^l Y_{lm}(\theta', \phi') \right] \cdot (\boldsymbol{r}' \times \boldsymbol{J}^p(\boldsymbol{r}')) \, \mathrm{d}^3 r'. \tag{84}$$

Hence, the multipole moments in the case of a spherically symmetric head model are fully determined by the primary current density $\boldsymbol{J}^p$ (or equivalently, the primary magnetization $\boldsymbol{r}' \times \boldsymbol{J}^p$). The multipole expansion in this case becomes

$$\boldsymbol{B}(\boldsymbol{r}) = -\frac{\mu_0}{4\pi} \operatorname{Re} \sum_{l=1}^{\infty} \sum_{m=0}^{l} (\alpha_{lm} + \mathrm{i}\, \beta_{lm}) \nabla \left(\frac{Y_{lm}^*(\theta, \phi)}{r^{l+1}} \right). \tag{85}$$

The result in (85) can also be derived from a spherical expansion of the radial field B_r (Haberkorn, 1994). Moreover, it has been shown that the dyadic multipole expansion of the magnetic field for an *infinite homogeneous* conductor is (Grynszpan and Geselowitz, 1973, Haberkorn, 1994)

$$\begin{aligned} \boldsymbol{B}^{inf}(\boldsymbol{r}) = {} & \frac{\mu_0}{4\pi} \operatorname{Re} \sum_{l=1}^{\infty} \sum_{m=0}^{l} (A_{lm} + \mathrm{i}\, B_{lm}) \nabla \left(\frac{Y_{lm}^*(\theta, \phi)}{n\, r^{l+1}} \right) \times \boldsymbol{r} \\ & - \frac{\mu_0}{4\pi} \operatorname{Re} \sum_{l=1}^{\infty} \sum_{m=0}^{l} (\alpha_{lm} + \mathrm{i}\, \beta_{lm}) \nabla \left(\frac{Y_{lm}^*(\theta, \phi)}{r^{l+1}} \right) \end{aligned} \tag{86}$$

where α_{lm} and β_{lm} are the magnetic moments defined in (84) and A_{lm} and B_{lm} are the electric moments defined by

$$A_{lm} + \mathrm{i}\, B_{lm} = \gamma_{l,m} \int_{v'} \nabla' \left[r'^l Y_{lm}(\theta', \phi') \right] \cdot \boldsymbol{J}^p(\boldsymbol{r}') \, \mathrm{d}^3 r'. \tag{87}$$

Comparing the magnetic field outside a spherically symmetric conductor (85) to the field of an infinite homogeneous conductor (86) leads to an interesting observation: the magnetic

field contribution of the *electric* multipoles and the contribution arising from the spherically symmetric conducting medium cancel each other out. It is therefore possible to expand the full magnetic field $\boldsymbol{B}$ outside a spherically symmetric conductor uniquely in terms of magnetic moments. Equation (85) provides such an expansion.

4.4. Radially oriented MEG sensor configuration

Finally, as in the previous section, we consider only the radial component of the magnetic field, using the developments of this section. A spherical multipole expansion of the radial field component $B_r(\boldsymbol{r}) = \boldsymbol{B}(\boldsymbol{r}) \cdot \boldsymbol{e}_r$ is easily obtained, using the general result in (82) and the relationship $-\nabla\big(Y_{lm}^* r^{-(l+1)}\big) \cdot \boldsymbol{e}_r = (l+1) Y_{lm}^* r^{-(l+2)}$, leading to

$$B_r(\boldsymbol{r}) = \frac{\mu_0}{4\pi} \operatorname{Re} \sum_{l=1}^{\infty} \sum_{m=0}^{l} (l+1)\, M_{lm} \left(\frac{Y_{lm}^*(\theta, \phi)}{r^{l+2}} \right) \tag{88}$$

where the multipole moments are generally defined by (80). However, if the volume conductor is assumed to be spherically symmetrical and centred at the origin of the coordinate system, then the moments depend only on the primary current density and are thus given by (84).

The spherical expansions and the related multipole moments of order l derived in the above sections for different volume conductors are summarized in table 2.

Table 2. The spherical harmonic multipole expansion of the full magnetic field and of its radial component outside a bounded volume conductor.

Full expansion	$\boldsymbol{B}(\boldsymbol{r}) = -\frac{\mu_0}{4\pi} \operatorname{Re} \sum_{l=1}^{\infty} \sum_{m=0}^{l} M_{lm} \nabla\big(\frac{Y_{lm}^*(\theta,\phi)}{r^{l+1}}\big)$
Radial expansion	$B_r(\boldsymbol{r}) = \frac{\mu_0}{4\pi} \operatorname{Re} \sum_{l=1}^{\infty} \sum_{m=0}^{l} (l+1)\, M_{lm} \big(\frac{Y_{lm}^*(\theta,\phi)}{r^{l+2}}\big)$

Volume conductor	Spherical multipole moments
Inhomogeneous	$M_{lm} = \frac{\gamma_{l,m}}{l+1} \int_{v'} \nabla' \big[r'^l Y_{lm}(\theta', \phi') \big] \cdot (\boldsymbol{r}' \times \boldsymbol{J}(\boldsymbol{r}'))\, \mathrm{d}^3 r'$
Piecewise homogeneous	$M_{lm} = \frac{\gamma_{l,m}}{l+1} \int \nabla' \big[r'^l Y_{lm}(\theta', \phi') \big] \cdot \boldsymbol{r}' \times \Big[\boldsymbol{J}^p(\boldsymbol{r}')\, \mathrm{d}^3 r' - \sum_{ij} (\sigma_i - \sigma_j) V(\boldsymbol{r}')\, \mathrm{d}\boldsymbol{S}'_{ij} \Big]$
Spherically symmetric	$M_{lm} = \frac{\gamma_{l,m}}{l+1} \int_{v'} \nabla' \big[r'^l Y_{lm}(\theta', \phi') \big] \cdot (\boldsymbol{r}' \times \boldsymbol{J}^p(\boldsymbol{r}'))\, \mathrm{d}^3 r'$

5. MME in Cartesian coordinates

It is often desirable to tackle multipole expansion problems using Cartesian tensors because the derivations for the dipolar and quadrupolar terms are elementary and the Cartesian multipole moments are easier to visualize. In inverse modelling, the translational invariance of the Cartesian coordinates simplifies the construction of multiple source models. We will therefore focus our discussion on the derivation of the MME in Cartesian coordinates by first considering the general case of Cartesian multipole expansions assuming an arbitrary volume conductor. Next, we present the general equations needed for the special case of a spherically symmetric head model followed by the MME of the radial field component.

5.1. Arbitrary volume conductor

Maxwell's equations for the quasi-static magnetic field $\boldsymbol{B}(\boldsymbol{r})$ due to a localized current distribution $\boldsymbol{J}$ are

$$\nabla \times \boldsymbol{B}(\boldsymbol{r}) = \mu_0 \boldsymbol{J}(\boldsymbol{r}) \tag{89}$$

$$\nabla \cdot \boldsymbol{B}(\boldsymbol{r}) = 0. \tag{90}$$

Taking the curl of (89) and using the identity $\nabla \times (\nabla \times \boldsymbol{P}) = \nabla(\nabla \cdot \boldsymbol{P}) - \nabla^2 \boldsymbol{P}$ and (90) we get the Poisson equation for the magnetostatic field

$$\nabla^2 \boldsymbol{B}(\boldsymbol{r}) = -\mu_0 \nabla \times \boldsymbol{J}(\boldsymbol{r}). \tag{91}$$

By analogy to (1) and (2), the solution of (91) is given by

$$\boldsymbol{B}(\boldsymbol{r}) = \frac{\mu_0}{4\pi} \int \frac{\nabla' \times \boldsymbol{J}(\boldsymbol{r}')}{|\boldsymbol{r} - \boldsymbol{r}'|} \, \mathrm{d}^3 r'. \tag{92}$$

The radial component is thus indirectly described by the scalar

$$\boldsymbol{r} \cdot \boldsymbol{B}(\boldsymbol{r}) = \frac{\mu_0}{4\pi} \int \frac{\boldsymbol{r} \cdot \nabla' \times \boldsymbol{J}(\boldsymbol{r}')}{|\boldsymbol{r} - \boldsymbol{r}'|} \, \mathrm{d}^3 r'. \tag{93}$$

Although we can use the above expression to obtain a multipole expansion of the magnetic scalar potential defined in (71), an alternative expression for $\boldsymbol{r} \cdot \boldsymbol{B}(\boldsymbol{r})$ presented by Gray (1979) is better suited for the multipole expansion. Consider the scalar product of the Poisson equation (91) with $\boldsymbol{r}$,

$$\boldsymbol{r} \cdot \nabla^2 \boldsymbol{B}(\boldsymbol{r}) = -\mu_0 \, \boldsymbol{r} \cdot \nabla \times \boldsymbol{J}(\boldsymbol{r}). \tag{94}$$

Given the general identity (e.g. Jackson 1975, p 744) $\boldsymbol{r} \cdot (\nabla^2 \boldsymbol{P}) = \nabla^2 (\boldsymbol{r} \cdot \boldsymbol{P}) - 2\nabla \cdot \boldsymbol{P}$, (94) becomes

$$\nabla^2 (\, \boldsymbol{r} \cdot \boldsymbol{B}(\boldsymbol{r})) = -\mu_0 \, \boldsymbol{r} \cdot \nabla \times \boldsymbol{J}(\boldsymbol{r}). \tag{95}$$

The solution of this Poisson equation is given by

$$\boldsymbol{r} \cdot \boldsymbol{B}(\boldsymbol{r}) = \frac{\mu_0}{4\pi} \int \frac{\boldsymbol{r}' \cdot \nabla' \times \boldsymbol{J}(\boldsymbol{r}')}{|\boldsymbol{r} - \boldsymbol{r}'|} \, \mathrm{d}^3 r' \tag{96}$$

Equations (93) and (96) are alternative equations for the same scalar quantity $\boldsymbol{r} \cdot \boldsymbol{B}$. At first glance, comparing these equations might lead to a suspicion of inconsistency; however, an alternative derivation of (96) starting from (93) clarifies the relationship and confirms the result (appendix B). The integrand in (96) is now a relatively simple function of $\boldsymbol{r}$, and we can easily expand this function. Using the property $\boldsymbol{r} \cdot \nabla \times \boldsymbol{J} = -\nabla \cdot (\boldsymbol{r} \times \boldsymbol{J})$ and inserting the Taylor expansion of Green's function as given by (13) into (96) yields

$$\begin{aligned} \boldsymbol{r} \cdot \boldsymbol{B}(\boldsymbol{r}) \simeq & -\frac{\mu_0}{4\pi} \left[\int [\nabla \cdot (\boldsymbol{r}' \times \boldsymbol{J}(\boldsymbol{r}'))] \, \mathrm{d}^3 r' \right] \frac{1}{r} \\ & + \frac{\mu_0}{4\pi} \left[\int [\nabla \cdot (\boldsymbol{r}' \times \boldsymbol{J}(\boldsymbol{r}'))] \, \boldsymbol{r}' \, \mathrm{d}^3 r' \right] \cdot \nabla \left(\frac{1}{r} \right) \\ & - \frac{\mu_0}{4\pi} \left[\frac{1}{2} \int [\nabla \cdot (\boldsymbol{r}' \times \boldsymbol{J}(\boldsymbol{r}'))] \, \boldsymbol{r}' \boldsymbol{r}' \, \mathrm{d}^3 r' \right] : \nabla \nabla \left(\frac{1}{r} \right). \end{aligned} \tag{97}$$

The first term in (97), which represents the contribution of the monopole, vanishes because the integral vanishes when the Gauss theorem is applied. Therefore

$$\boldsymbol{r} \cdot \boldsymbol{B}(\boldsymbol{r}) = \frac{\mu_0}{4\pi} \left[-2 \, \boldsymbol{m} \cdot \nabla \left(\frac{1}{r} \right) + \boldsymbol{Q}_M : \nabla \nabla \left(\frac{1}{r} \right) + \cdots \right] \tag{98}$$

where the vector $\boldsymbol{m}$ is the magnetic dipole moment defined by

$$\boldsymbol{m} = -\frac{1}{2}\int [\nabla \cdot (\boldsymbol{r}' \times \boldsymbol{J}(\boldsymbol{r}'))]\, \boldsymbol{r}'\, \mathrm{d}^3 r' = \frac{1}{2}\int \boldsymbol{r}' \times \boldsymbol{J}(\boldsymbol{r}')\, \mathrm{d}^3 r' \tag{99}$$

and the tensor $\boldsymbol{Q}_M$ is the magnetic quadrupole moment defined by

$$\boldsymbol{Q}_M = -\frac{1}{2}\int [\nabla \cdot (\boldsymbol{r}' \times \boldsymbol{J}(\boldsymbol{r}'))]\, \boldsymbol{r}'\boldsymbol{r}'\, \mathrm{d}^3 r' = \frac{1}{2}\int (\boldsymbol{r}' \times \boldsymbol{J}(\boldsymbol{r}')) \cdot \nabla' (\boldsymbol{r}'\boldsymbol{r}')\, \mathrm{d}^3 r'. \tag{100}$$

Using (69) and noting that $r\frac{\partial}{\partial r} r^{-(l+1)} = -(l+1) r^{-(l+1)}$, we substitute this relation into each term of (98) to yield the magnetic scalar potential V_m (Gray 1979),

$$V_m(\boldsymbol{r}) = \frac{1}{4\pi}\left[-\boldsymbol{m} \cdot \nabla \left(\frac{1}{r}\right) + \frac{1}{3}\boldsymbol{Q}_M : \nabla\nabla \left(\frac{1}{r}\right) + \cdots \right]. \tag{101}$$

where $V_m(\infty) = 0$. Finally using $\boldsymbol{B} = -\mu_0 \nabla V_m$ we obtain the multipole expansion for the full magnetic field (Gray 1979),

$$\boldsymbol{B}(\boldsymbol{r}) = \frac{\mu_0}{4\pi}\left[\boldsymbol{m} \cdot \nabla\nabla \left(\frac{1}{r}\right) - \frac{1}{3}\boldsymbol{Q}_M : \nabla\nabla\nabla \left(\frac{1}{r}\right) + \cdots \right] \tag{102}$$

where the magnetic dipole and quadrupole moments are respectively defined by (99) and (100). Two alternative approaches to the Cartesian expansion of the magnetic field outside a localized source are found in Castellanos *et al* (1978) and more recently in Gonzalez *et al* (1997).

5.2. Properties of the magnetic quadrupole moment

In this section we examine the trace and symmetry properties of $\boldsymbol{Q}_M$. The trace $\mathrm{Tr}(\boldsymbol{Q}) \equiv \sum_\alpha Q_{\alpha\alpha}$ is given by

$$\mathrm{Tr}(\boldsymbol{Q}_M) = \frac{1}{2}\int (\boldsymbol{r}' \times \boldsymbol{J}(\boldsymbol{r}')) \cdot \nabla' r'^2\, \mathrm{d}^3 r' = \frac{1}{2}\int (\boldsymbol{r}' \times \boldsymbol{J}(\boldsymbol{r}')) \cdot (-2\,\boldsymbol{r}')\, \mathrm{d}^3 r' = 0. \tag{103}$$

Thus the quadrupolar moment $\boldsymbol{Q}_M$ is a traceless tensor. Moreover, (100) can be transformed into the form (Gray 1979),

$$\boldsymbol{Q}_M = \frac{1}{2}\int (\boldsymbol{r}' \times \boldsymbol{J}(\boldsymbol{r}'))\, \boldsymbol{r}' + \boldsymbol{r}'(\boldsymbol{r}' \times \boldsymbol{J}(\boldsymbol{r}'))\, \mathrm{d}^3 r'. \tag{104}$$

From this form of the tensor we see that $Q_{M\alpha\beta} = Q_{M\beta\alpha}$, and therefore $\boldsymbol{Q}_M$ is also symmetric.

The implications of these properties are best understood by considering the portion of the field that arises from the quadrupolar term. This contribution can be identified in (98) as being

$$\boldsymbol{Q}_M : \boldsymbol{T}(\boldsymbol{r}) \tag{105}$$

where we define

$$\boldsymbol{T}(\boldsymbol{r}) = \nabla\nabla \left(\frac{1}{r}\right) = \left(\frac{3\,\boldsymbol{r}\boldsymbol{r} - \boldsymbol{I}r^2}{r^5}\right). \tag{106}$$

Consequently the tensor components are given by

$$\boldsymbol{T}_{ij} = \frac{3\, r_i r_j - \delta_{ij} r^2}{r^5}. \tag{107}$$

It is now easy to see that $\boldsymbol{T}_{ij} = \boldsymbol{T}_{ji}$ and $\sum_{i=1}^{3} \boldsymbol{T}_{ii} = 0$. The tensor $\boldsymbol{T}$ is therefore both symmetric and traceless. As a result, only the traceless symmetric part of any definition of the quadrupole moment $\boldsymbol{Q}_M$ will survive the contraction $\boldsymbol{Q}_M : \boldsymbol{T}$ because

$$\boldsymbol{A} : \boldsymbol{B} = \boldsymbol{A}^t : \boldsymbol{B}^t + \boldsymbol{A}^a : \boldsymbol{B}^a + \boldsymbol{A}^{ts} : \boldsymbol{B}^{ts} \tag{108}$$

Table 3. The Cartesian MME about the origin of the coordinate system. For a spherically symmetric conductor centred at the origin of the coordinate system, the same equations remain valid if we replace $\boldsymbol{J}$ by $\boldsymbol{J}^p$.

Full expansion	$\boldsymbol{B}(\boldsymbol{r}) = \frac{\mu_0}{4\pi}\left[\boldsymbol{m}\cdot\nabla\nabla\left(\frac{1}{r}\right) - \frac{1}{3}\boldsymbol{Q}_M : \nabla\nabla\nabla\left(\frac{1}{r}\right) + \cdots\right]$
Radial expansion	$B_r(\boldsymbol{r}) = \frac{\mu_0}{4\pi}\left[\frac{2\boldsymbol{m}\cdot\boldsymbol{r}}{r^4} + \boldsymbol{Q}_M : \left(\frac{3\,\boldsymbol{r}\boldsymbol{r} - \boldsymbol{I}\,r^2}{r^6}\right) + \cdots\right]$

Moment	Definition	Properties
Dipole	$\boldsymbol{m} = \frac{1}{2}\int \boldsymbol{r}' \times \boldsymbol{J}(\boldsymbol{r}')\,\mathrm{d}^3 r'$	Origin independent
Quadrupole	$\boldsymbol{Q}_M = \frac{1}{2}\int (\boldsymbol{r}' \times \boldsymbol{J}(\boldsymbol{r}'))\boldsymbol{r}' + \boldsymbol{r}'(\boldsymbol{r}' \times \boldsymbol{J}(\boldsymbol{r}'))\,\mathrm{d}^3 r'$	Traceless, symmetric
	$\boldsymbol{Q}'_M = \int (\boldsymbol{r}' \times \boldsymbol{J}(\boldsymbol{r}'))\,\boldsymbol{r}'\,\mathrm{d}^3 r'$	Traceless, asymmetric

where $\boldsymbol{A}^t$, $\boldsymbol{A}^a$ and $\boldsymbol{A}^{ts}$ are the trace, antisymmetric and traceless symmetric parts of $\boldsymbol{A}$ respectively (Gray 1980).

Now, since $\boldsymbol{T}$ is symmetric the two terms arising from $(\boldsymbol{r}' \times \boldsymbol{J}(\boldsymbol{r}'))\boldsymbol{r}'$ and from $\boldsymbol{r}'(\boldsymbol{r}' \times \boldsymbol{J}(\boldsymbol{r}'))$ in (104) will contribute equally to the external field. We can therefore define a new quadrupole moment $\boldsymbol{Q}'_M$ such that

$$\boldsymbol{Q}'_M = \int (\boldsymbol{r}' \times \boldsymbol{J}(\boldsymbol{r}'))\,\boldsymbol{r}'\,\mathrm{d}^3 r'. \tag{109}$$

or another in terms of $\boldsymbol{r}'(\boldsymbol{r}' \times \boldsymbol{J}(\boldsymbol{r}'))$. The moment $\boldsymbol{Q}'_M$ is not generally symmetric and is thus not equal to $\boldsymbol{Q}_M$ in general, although it does have the same field contribution. The main difference is that $\boldsymbol{Q}'_M$ has eight independent components whereas $\boldsymbol{Q}_M$ has five. A related issue is that a non-symmetric $\boldsymbol{Q}'_M$ may not have physical principal axes, unlike the case for symmetric source distributions (Gray 1980).

The important observation here is that only the traceless symmetric part of the moment tensor contributes to the overall field. Thus, from the perspective of solving inverse problems, a non-unique relationship exists between any particular magnetic field and the quadrupolar component of the best fitting truncated multipole expansion. Consequently, to avoid this ambiguity, we may apropriately restrict the definition of the moments to be traceless and symmetric when using these expansions in solving the MEG inverse problem.

5.3. Spherically symmetric head model

For the case of a spherically homogeneous conductor centred on the origin, as in section 4.3, we may replace the total current density $\boldsymbol{J}$ with just the primary current density $\boldsymbol{J}^p$. The dipolar and quadrupolar moments of the magnetic multipole expansion outside a spherically symmetric conductor are given by

$$\boldsymbol{m} = \frac{1}{2}\int \boldsymbol{r}' \times \boldsymbol{J}^p(\boldsymbol{r}')\,\mathrm{d}v' \tag{110}$$

and

$$\boldsymbol{Q}_M = \frac{1}{2}\int (\boldsymbol{r}' \times \boldsymbol{J}^p(\boldsymbol{r}'))\boldsymbol{r}' + \boldsymbol{r}'(\boldsymbol{r}' \times \boldsymbol{J}^p(\boldsymbol{r}'))\,\mathrm{d}v'. \tag{111}$$

A full multipole expansion of the magnetic field outside a spherically symmetric conductor for a source placed at the origin of the coordinate system is thus given by inserting (110) and (111) into (102). The expansions for a spherically symmetric head model can be immediately obtained from the equations in table 3 by substituting $\boldsymbol{J}^p$ for $\boldsymbol{J}$.

5.4. Radially oriented MEG sensors

The Cartesian expansion of the radial magnetic field about the origin of the coordinate system can be obtained from (98) by first computing the gradients as in (14) and then scaling by $1/r$ to yield

$$B_r(\boldsymbol{r}) = \frac{\mu_0}{4\pi}\left[\frac{2\boldsymbol{m}\cdot\boldsymbol{r}}{r^4} + \boldsymbol{Q}_M : \left(\frac{3\,\boldsymbol{r}\boldsymbol{r} - \boldsymbol{I}\,r^2}{r^6}\right) + \cdots\right] \tag{112}$$

where the moments are defined in (99) and (100). If the volume conductor is spherically symmetric, the contribution of the volume currents to the radial field vanishes. In this case the moments are given in (110) and (111).

5.5. MME about an arbitrary location

The above expansions are centred on the origin and as such converge geometrically at the rate of r'/r. The multipole series converges faster if the expansion point is near the centroid of the primary current region rather than at the origin of the coordinate system. Consequently, we are interested in using multipole expansions computed about an arbitrary location.

The MME of the full magnetic field about the origin of the coordinate system is given by equation (102) and its magnetic moments are defined in (99) and (100). Because this MME is valid for an arbitrary Cartesian coordinate system, we may write the multipole expansion of the same field in a translated coordinate system centred at $\boldsymbol{l}$ with the coordinate $\boldsymbol{R} = \boldsymbol{r} - \boldsymbol{l}$. Denoting the magnetic field and the current density in the new coordinate system by $\boldsymbol{B}_l(\boldsymbol{R})$ and $\boldsymbol{J}_l(\boldsymbol{R})$ we have

$$\boldsymbol{B}_l(\boldsymbol{R}) = \boldsymbol{B}(\boldsymbol{R}+\boldsymbol{l}) = \boldsymbol{B}(\boldsymbol{r}) \tag{113}$$

$$\boldsymbol{J}_l(\boldsymbol{R}) = \boldsymbol{J}(\boldsymbol{R}+\boldsymbol{l}) = \boldsymbol{J}(\boldsymbol{r}). \tag{114}$$

The MME in (102) may now be written in the new coordinate system as

$$\boldsymbol{B}_l(\boldsymbol{R}) = \frac{\mu_0}{4\pi}\left[\tilde{\boldsymbol{m}}\cdot\nabla\nabla\left(\frac{1}{R}\right) - \frac{1}{3}\,\tilde{\boldsymbol{Q}}_M : \nabla\nabla\nabla\left(\frac{1}{R}\right) + \cdots\right] \tag{115}$$

where the shifted magnetic dipole and quadrupole moments are respectively obtained by replacing $\boldsymbol{r}'$ with $\boldsymbol{R}'$ in (99) and (100), i.e.

$$\tilde{\boldsymbol{m}} = \frac{1}{2}\int \boldsymbol{R}' \times \boldsymbol{J}_l(\boldsymbol{R}')\,\mathrm{d}^3R' \tag{116}$$

$$\tilde{\boldsymbol{Q}}_M = \frac{1}{2}\int (\boldsymbol{R}' \times \boldsymbol{J}_l(\boldsymbol{R}'))\cdot\nabla'\,(\boldsymbol{R}'\boldsymbol{R}')\,\mathrm{d}^3R'. \tag{117}$$

Note that the derivatives ∇ and ∇' are taken with respect to $\boldsymbol{R}$ and $\boldsymbol{R}'$ respectively and that, similar to the CME section, the notation $\tilde{\boldsymbol{m}}$ and $\tilde{\boldsymbol{Q}}_M$ is used to distinguish moments computed about a new expansion point from those obtained with the same source if computed about the origin of an initial coordinate system and denoted by $\boldsymbol{m}$ and $\boldsymbol{Q}_M$.

Finally, if we transform the expansion back to the original coordinate system using the relationships in (113) and (114), we obtain the full field $\boldsymbol{B}$ expanded about an arbitrary point $\boldsymbol{l}$,

$$\boldsymbol{B}(\boldsymbol{r}) = \frac{\mu_0}{4\pi}\left[\tilde{\boldsymbol{m}}\cdot\nabla\nabla\left(\frac{1}{|\boldsymbol{r}-\boldsymbol{l}|}\right) - \frac{1}{3}\,\tilde{\boldsymbol{Q}}_M : \nabla\nabla\nabla\left(\frac{1}{|\boldsymbol{r}-\boldsymbol{l}|}\right) + \cdots\right] \tag{118}$$

where the moments are respectively defined by

$$\tilde{\boldsymbol{m}} = \frac{1}{2}\int ((\boldsymbol{r}'-\boldsymbol{l})\times\boldsymbol{J}(\boldsymbol{r}'))\,\mathrm{d}^3r' = \frac{1}{2}\int (\boldsymbol{r}'\times\boldsymbol{J}(\boldsymbol{r}'))\,\mathrm{d}^3r' = \boldsymbol{m} \tag{119}$$

and

$$\tilde{\boldsymbol{Q}}_M = \frac{1}{2}\int ((\boldsymbol{r}' - \boldsymbol{l}) \times \boldsymbol{J}(\boldsymbol{r}')) \cdot \nabla' ((\boldsymbol{r}' - \boldsymbol{l})(\boldsymbol{r}' - \boldsymbol{l}))\, \mathrm{d}^3 r'. \tag{120}$$

The magnetic moments in (119) and (120) are given in terms of the magnetization centred about an arbitrary point $\boldsymbol{l}$; therefore, the volume currents in a conductor that is spherically symmetric about the origin do not readily cancel in the higher order moments. The MME in (118) is limited to problems that can be solved in terms of the total current density. In contrast, defining the source term to be the magnetization about the origin $\boldsymbol{r}' \times \boldsymbol{J}(\boldsymbol{r}')$ and expanding the kernel using a Taylor series expansion about $\boldsymbol{l}$ yields a less conventional and more complicated MME expression. In this case, however, in a conductor of homogeneous spherical symmetry, we can again neglect the volume currents, yielding an MME expressed in terms of primary magnetization currents only (Mosher *et al* 1999a, 1999b, 2000), analogous to the CME expression developed in section 3.4. While this reduction to primary currents is a strong advantage, the higher order moments now depend on both the coordinate system and the expansion point.

6. Simulations

6.1. Current multipole unit fields

We investigate properties of the CME of the radial magnetic field by considering the field patterns produced by the dipolar and quadrupolar components of the expansion. The volume conductor is assumed to be spherically homogeneous about an origin, such that we need only consider the primary currents in our formulas. For further simplification in the exposition, we arranged all sensors radially, with the result that (46) is the relatively simple CME model for these dipolar and quadrupolar fields. Truncating the CME of the radial component of the MEG field after the quadrupolar term leads to the truncated expansion given in (47),

$$B_r(\boldsymbol{r}) = \frac{\mu_0}{4\pi}\boldsymbol{k}_D \cdot \boldsymbol{q} + \frac{\mu_0}{4\pi}\boldsymbol{k}_Q : \tilde{\boldsymbol{Q}}_E$$

where the three-dimensional vector $\boldsymbol{k}_D$ and the 3×3 tensor $\boldsymbol{k}_Q$ are defined by (48) and (49) respectively.

We consider a simulated array of m sensors arranged on a spherical half-shell at a distance of 12 cm from the origin. The set of measurements is arranged in an m-dimensional vector and we define the $m \times 3$ dipolar gain matrix K_D as the concatenation of the vectors $\boldsymbol{k}_D$ evaluated at m different sensors on a spherical sensor array. In other words, each row of K_D is the evaluation of $\boldsymbol{k}_D$ at a different sensor location. Similarly, the lexicographical ordering and concatenation of the 3×3 tensors $\boldsymbol{k}_Q$ leads to the $m \times 9$ quadrupolar gain matrix K_Q.

Since the measurements are on a virtual hemispherical surface, the measurements can be interpolated on this surface to yield continuous topographic maps. In the figures that follow, we view decompositions of these topographic maps from directly above the hemisphere. Each column of the gain matrices represents a topography for a particular component of the moments and plots of the three columns of K_D and the nine columns of K_Q yield partly redundant patterns. These redundancies can be eliminated by plotting a lower rank set of unit fields that span the column space of the gain matrices. A *singular value decomposition* (SVD) of K_D and K_Q yields unit orthogonal topographies that sum together to create any possible observable topography. We denote the SVD of each matrix as

$$K_D = U_D \Sigma_D V_D^T \qquad K_Q = U_Q \Sigma_Q V_Q^T \tag{121}$$

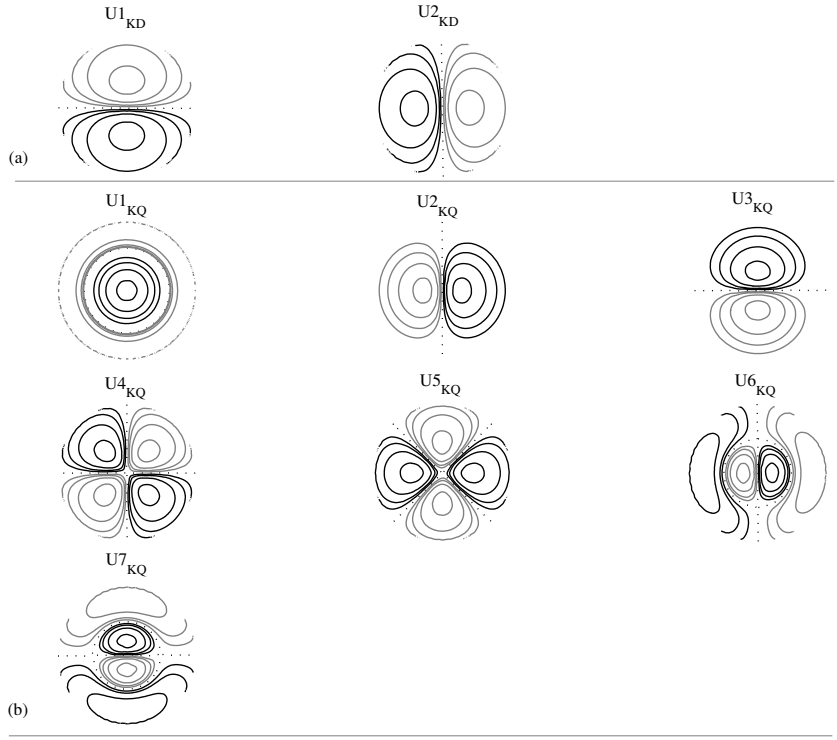

Figure 3. Three-dimensional topographies for the current multipole expansion of (a) the first two singular vectors of U_D obtained from the SVD of the dipolar gain matrix K_D and (b) of the first seven singular vectors of U_Q obtained by SVD of the quadrupolar gain matrix K_Q, for an expansion point centred on the z-axis at $\boldsymbol{l} = (0, 0, 70)$ mm and assuming a hemispherical array of $m = 138$ radial sensors at 120 mm from the centre of the sphere. The measurements are interpolated onto the surface of the hemisphere, contoured and viewed from above. Consecutive isocontours differ by a factor of two. Dotted lines represent zero-crossings.

where the columns of the orthogonal matrices U and V contain the *left* and *right singular vectors* respectively and $\mathrm{diag}(\Sigma) = \sigma_1, \sigma_2, \ldots$, are the *singular values* ordered in descending order (Golub and van Loan, 1989). The number k of strictly non-zero singular values determines the *rank* of the matrix, and we will use the convention that SVD yields only those components that correspond to the rank of the matrix, i.e. the SVD of an $m \times n$ matrix of rank k yields U of dimension $m \times k$, Σ is $k \times k$, and V is $n \times k$.

Given that the contributions of radially oriented current dipoles vanish, K_D has a rank of two. The SVD of K_Q reveals that it is of rank seven and contains, in its column space, the two-dimensional subspace spanned by the columns of K_D. The columns of the matrices U_D (rank two) and U_Q (rank seven) are the singular vectors that correspond to the non-zero singular values. Each singular vector may be viewed as a basis component in an orthogonal decomposition of the measurement vector and we may view each singular vector as a virtual topography by interpolating its values onto the simulated hemispherical measurement surface. We consider the particular case of a current multipole located at $\boldsymbol{l} = (0, 0, 70)$ mm, which results in the orthogonal topographies shown in figures 3(a) and (b) respectively.

Since the rank seven quadrupolar subspace U_Q also contains the rank two dipolar subspace U_D, it is convenient for viewing purposes to reduce U_Q to a rank five subspace using the

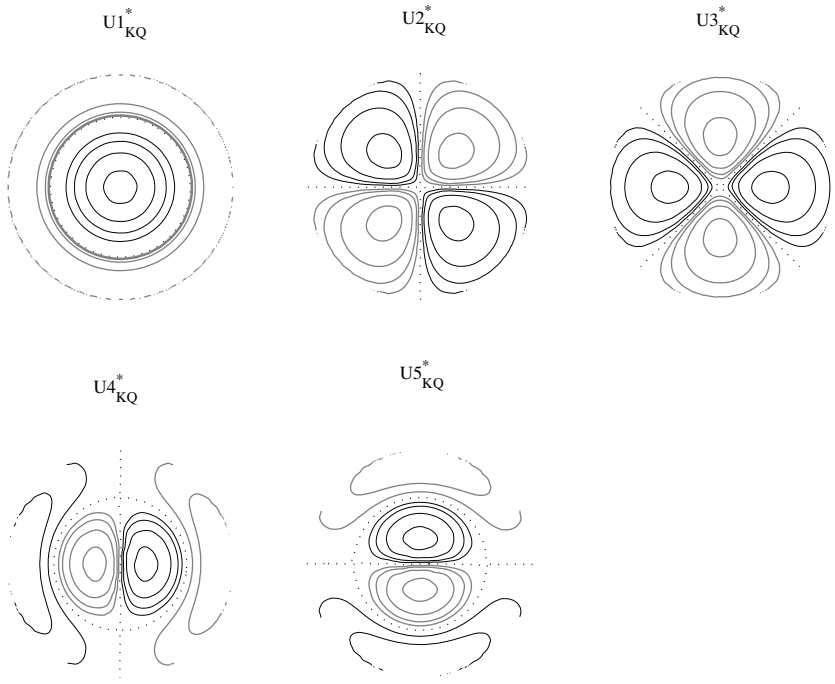

Figure 4. Three-dimensional topographies of the first five singular vectors of U_Q^* obtained after an orthogonal projection of K_Q away from the dipolar gain matrix. Dotted lines represent zero-crossings.

orthogonal projection operator $P_D^{\perp} = \boldsymbol{I} - U_D U_D^T$, where $\boldsymbol{I}$ is the identity matrix, such that $P_D^{\perp} K_Q$ projects the quadrupolar subspace away from the space spanned by K_D. Applying the orthogonal projection yields the rank five matrix K_Q^* defined by

$$K_Q^* = P_D^{\perp} K_Q. \tag{122}$$

The five-unit field patterns of the left singular vectors of U_Q^*, obtained from the SVD of K_Q^*, are shown in figure 4. By construction, the patterns in figures 3(a) and 4 are orthogonal to one another. The combination of these independent field topographies can be viewed as a spatial basis of the multipole model.

6.2. Spatially extended sources

In order to assess the utility of the proposed multipolar approach from a forward modelling standpoint, we used clusters of *elemental dipoles* to simulate spatially extended neural sources. We then qualitatively and quantitatively compared the fields generated by these extended sources with those of the multipolar model above, investigating the degree of dipolarity and the contributions of the higher order field patterns.

An elemental dipole can be viewed as a very small volume of primary current activity and integrating this volume yields an elemental dipole moment $\boldsymbol{q}_i$ for the ith volume. This moment and the centre of this small volume are then used in (48) to generate the contribution of each volume element to the measurement field. Thus a larger region of primary current density is partitioned into numerous adjacent elemental dipoles. Several two-dimensional and three-dimensional dipole clusters were created for this study. The orientation of each elemental dipole was left unconstrained. As in the above simulations, we continued to use a 120 mm

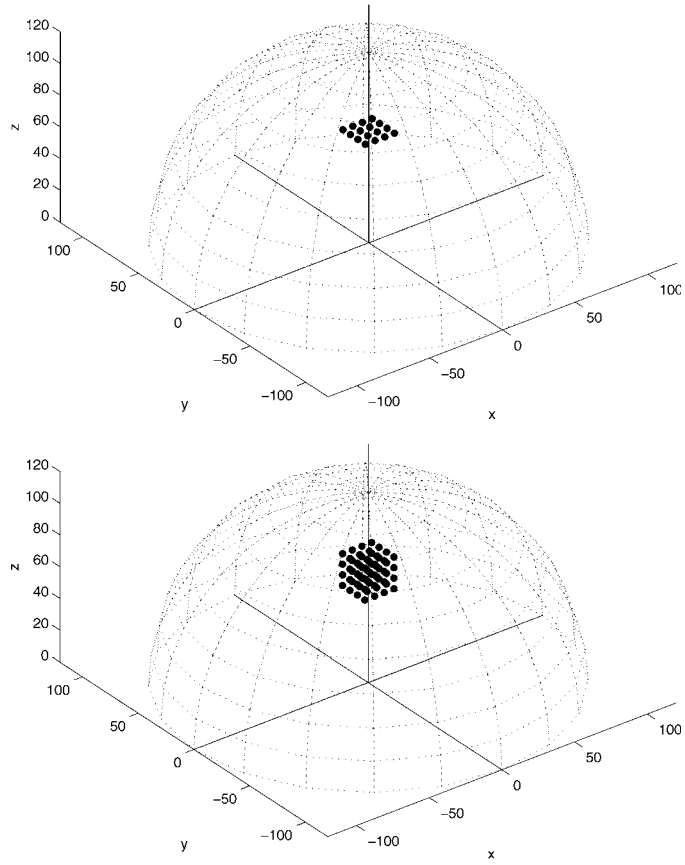

Figure 5. Examples of 2D (top) and 3D (bottom) clusters of dipoles. An elemental dipole is assigned to each grid point to simulate spatially extended areas of activation. Both the patch and the cube are centred at $\boldsymbol{l} = (0, 0, 70)$ mm. Sparse grids are shown to simplify the visualization. Denser grids (1–2 mm dipole spacing) were used in the simulations.

hemispherical array of radially oriented sensors and all dipole clusters were centred on the z-axis at $z = 70$ mm. The arrangement is illustrated in figure 5.

For m measurements, each elemental dipole may be represented by a $m \times 3$ gain matrix and the overall gain matrix G_{Cluster} of a patch or cube of dipoles is represented by superposition (concatenation) of the gain matrices for each elemental dipole in the grid into an overall $m \times 3p$ matrix, where p is the number of dipoles. As above, we can then perform an SVD of G_{Cluster} and examine the dominant singular values and their corresponding left and right singular vectors. The range of the singular values for several 2D and 3D clusters is shown in figure 6. In all cases, two equally strong singular values are followed by between five and seven additional weaker yet significant singular values. The significance of the k*th* singular value can be quantified by computing its percent energy contribution $e(k)$ to the overall matrix

$$e(k) = \sum_{i=1}^{k} \sigma_i^2 \Bigg/ \sum_{i=1}^{N} \sigma_i^2 \tag{123}$$

where N is the total number of singular values. This metric provides a convenient way of identifying how many of the singular values are needed for the description of the subspace

Table 4. Cumulative contributions $e(k)$ (in %) of the first nine singular values ($k = 1, \ldots, 9$) to the overall matrix energy for 2D and 3D clusters of dipoles of different dimensions. The rank of the first subspace that accounts for more than 99% of the energy is given in the last row. All patches were centred at (0, 0, 70) mm and had a 1 mm uniform dipole spacing.

	2D grid dimensions (cm)					3D cluster dimensions (cm)	
k	0.5×0.5	1×1	2×2	3×3	4×4	$1 \times 1 \times 1$	$2 \times 2 \times 2$
1	49.8%	49.32%	47.60%	45.02%	41.85%	49.17%	46.97%
2	99.60	98.64	95.19	90.04	83.69	98.34	93.94
3	99.84	99.46	98.02	95.74	92.64	99.16	96.88
4	99.92	99.73	98.98	97.71	95.85	99.44	97.89
5	100	99.99	99.90	99.55	98.73	99.71	98.86
6	100	99.99	99.93	99.70	99.13	99.85	99.35
7	100	100	99.97	99.84	99.52	99.99	99.83
8	100	100	99.98	99.91	99.71	99.99	99.89
9	100	100	100	99.98	99.90	99.99	99.92
rank	2	3	5	5	6	3	6

with a given accuracy (e.g. 99%). The results for several 2D and 3D clusters (table 4) clearly show that, for the 2D patches, the first five singular values already describe more than 99% of the total matrix energy of the patch. The contribution of the third, fourth and fifth component increases with the size of the patch, i.e. the spatial extent of the source, which we also observe in figure 6. Similar observations follow for the 3D patches.

The elemental dipoles were formed on a uniform 1 mm grid in all dimensions. We also investigated other grid densities by varying the dipole spacing up to 3 mm and we found that the effect of grid density on the singular values was very small compared to the effect caused by changing the dimensions of the cluster.

To investigate the magnetic field patterns that constitute the principal components in the SVDs and the current fields that produce them, we plotted the topographies associated with each of the first 12 left singular vectors U_i (i.e. columns of matrix U) for a cube of dipoles (figure 7). The first three topographies clearly represent current dipolar patterns in x-, y- and z-directions respectively. The next five topographies show typical quadrupolar patterns. The remaining topographies are octupolar and higher.

As described above, each set of three columns of G_{Cluster} corresponds to one of the elemental dipoles in the patch, and as such the right singular vectors V_i can be used to describe the orientation and strength of each of the dipoles needed to produce each of the field patterns shown in the corresponding left singular vectors. For a given right singular vector V_i, each set of three elements in the vector represents the orientation and magnitude of the corresponding elemental dipole in the patch. We can therefore plot 'arrows' of the corresponding orientations and lengths at the three-dimensional locations of all dipoles in a patch, thereby revealing the pattern of dipolar activity in three dimensions that gave rise to the particular topography.

In figure 8 we plot the first 12 right singular vectors for a 20×20 mm^2 two-dimensional patch of dipoles. The successive configurations clearly show standard dipolar, quadrupolar and higher order source patterns. Again, these figures support the use of multipolar models as a natural decomposition.

The SVD analysis of these clusters show two strong dipolar components, reflecting the high degree of dipolarity obtained by superimposing the effect of hundreds of elemental dipoles in a relatively small volume. This observation provides strong empirical support for the widespread use of equivalent current dipoles for representation of focal activation. The

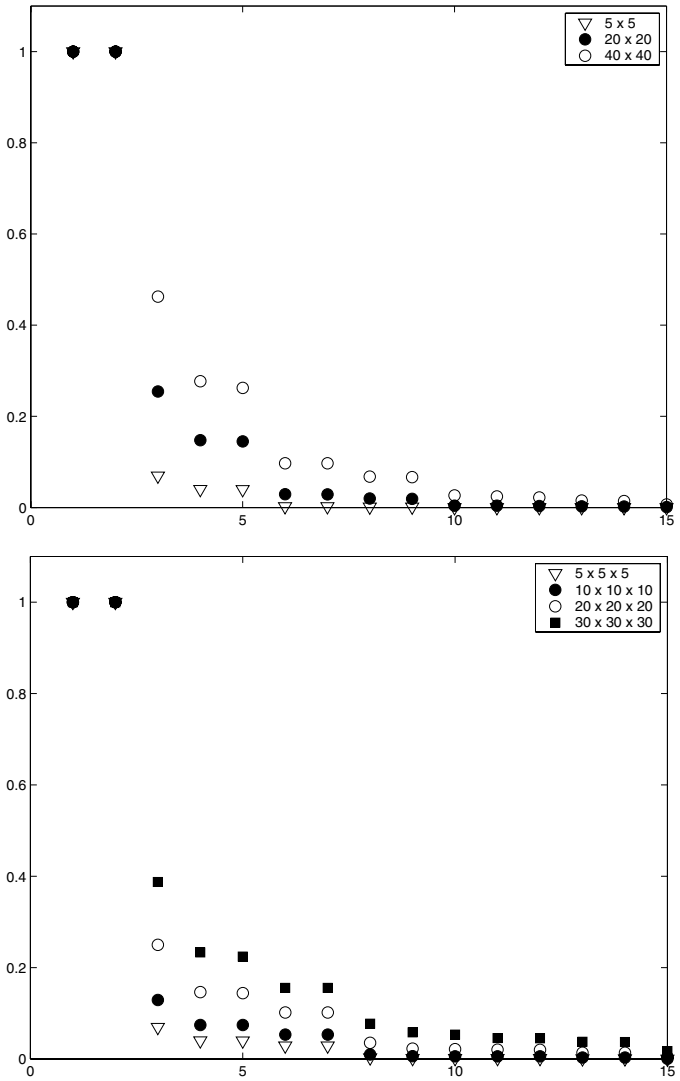

Figure 6. SVDs of clusters of dipoles centred at $(x, y, z) = (0, 0, 70)$ mm. Top: Singular value decay for patches of variable size (5×5 mm^2, 20×20 mm^2, 40×40 mm^2). Bottom: Singular value decay for cubes of dipoles ($5 \times 5 \times 5$ mm^3, $10 \times 10 \times 10$ mm^3, $20 \times 20 \times 20$ mm^3, $30 \times 30 \times 30$ mm^3).

topographies of the next singular vectors suggest that their contribution could be modelled by adding quadrupolar terms to the dipolar source. Indeed, the same field patterns we see in the first seven singular vector topographies in figure 7 match remarkably well with the unit fields of current dipoles and current quadrupoles shown in figures 3(a) and 4. These observations provide a strong graphical illustration for the argument that multipolar models are a rather natural approach to parametric representation of distributed current sources. As one might expect, the singular values show that the contribution of the higher order source pattern gains in importance when the size of the patch increases. Accordingly, including higher order source models such as quadrupoles or octupoles should lead to a better source description than simple dipoles for spatially extended sources.

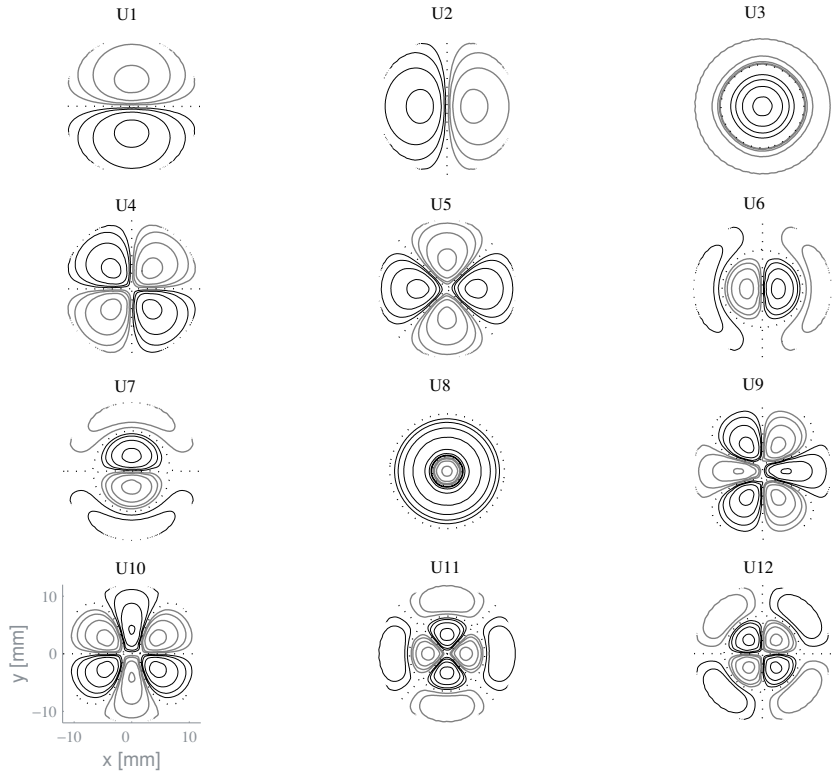

Figure 7. Topographies produced by the first 12 left singular vectors U_i for a $20 \times 20 \times 20$ mm^3 cube centered on the z-axis at $z = 70$ mm within a spherical head model on a spherical array of sensors at 12 cm from the centre of the head. Consecutive contours differ by a factor 2. Dotted lines represent zero-crossings.

The above analysis qualitatively displays the correspondence between the dominant current patterns in a patch of elemental dipoles and the multipolar models. To perform a quantitative comparison between the multipole models and these patches, we also computed the multipolar gain matrices K_D and K_Q for an expansion point at the centroid of these patches. We then computed the *principal angles* θ_i, $i = 1, \ldots, k$ (Golub and van Loan 1989) between the field pattern subspaces for the current multipole model and the patches; here k is the minimum of the ranks of the two matrices. The similarity between the two subspaces can be expressed in terms of the scalar distance metric (Golub and van Loan 1989)

$$\mathrm{dist}(G_{\mathrm{Cluster}}, G_{\mathrm{Model}}) = \sqrt{1 - \cos^2(\theta_k)}\ . \tag{124}$$

If the two matrices share a common subspace of dimension $n \leqslant \mathrm{k}$ then the first n principal angles will be zero. The distance between the two subspaces will be zero if one subspace completely contains the other. For the purposes of using multipole models to represent clusters of dipoles, it is desirable that the principal angles between the model and cluster gain matrices are approximately zero up to the effective dimension of the cluster gain matrix.

Since angles may range from zero to π, we find it more intuitive to view these angles in terms of a 'subspace correlation' metric defined simply as the cosine of the principal angle. Thus a subspace correlation of unity indicates perfect alignment between two dimensions, and a correlation of zero their orthogonality. In table 5 we show the subspace correlations for patches of various sizes compared with the current multipole gain (47), i.e. dipolar and

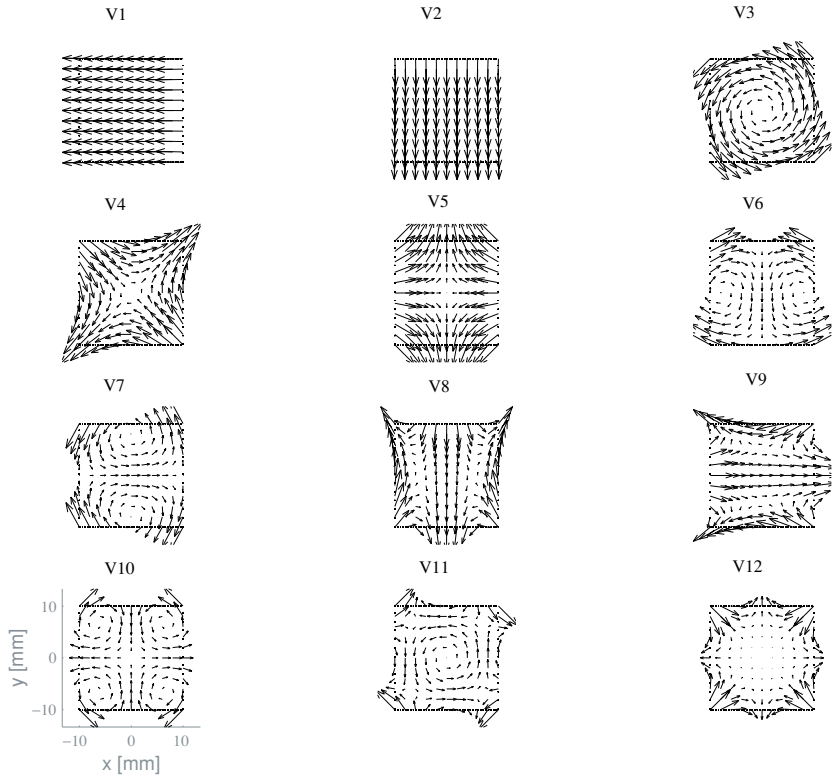

Figure 8. Plots of dipole orientations for the first 12 right singular vectors V_i for a 20×20 mm^2 patch centred at (0, 0, 70) mm within a spherical head model.

Table 5. The subspace correlations (cosine of the principal angles, $\cos\theta_i$)) between the multipolar source model and the cluster subspaces (rank i, where $i = 1, \ldots, k$). The distances (dist) between the relevant subspace of G_{Cluster} (rank k) and the multipole model are explicitly given in the last row. The 2D and 3D clusters of dipoles have variable effective dimensions and are all centred at $z = 70$ mm.

	2D patch dimensions (cm)					3D patch dimensions (cm)	
i	0.5×0.5	1×1	2×2	3×3	4×4	$1 \times 1 \times 1$	$2 \times 2 \times 2$
1	1.0	1.0	1.0	0.9999	0.9997	1.0	1.0
2	1.0	1.0	1.0	0.9999	0.9997	1.0	1.0
3	–	1.0	0.9997	0.9991	0.9975	1.0	1.0
4	–	–	0.9996	0.9985	0.9957	–	1.0
5	–	–	0.9991	0.9965	0.9909	–	1.0
6	–	–	–	–	0.8755	–	0.9999
k	2	3	5	5	6	3	6
dist	0.0	0.0	0.04	0.08	0.48	0.0	0.01

quadrupolar terms. These values should be interpreted in light of the results in table 4, since the values of the principal angles are only of interest up to the effective dimension of the subspace. We chose k in (124) to be the effective rank of the relevant subspace, i.e. the subspace of the patch that describes 99% of the total energy of the patch.

Due to the redundancies among K_D and K_Q, the CM model is effectively rank seven (two dipolar plus five quadrupolar terms). The subspace correlation results in table 5 demonstrate that the relevant subspace (rank k) of the patches is successfully matched (dist $\simeq 0$) by the multipole model in all of the cases shown except for the 4×4 cm patch. In this particular case, the source is so large (16 cm^2) that a high subspace correlation up to the sixth dimension is needed to describe more than 99% of the total patch energy, yet the multipole model achieves good correlations up to only the fifth dimension. This one exception does not limit the proposed use of the CME model truncated at the quadrupolar term because we realistically expect many of the extended sources of interest in the human brain to be smaller than 16 cm^2.

Generally, we found that the multipolar model achieves high subspace correlations up to rank five for the 2D patches and up to rank seven in the 3D clusters. In contrast, the classical ECD model only matches the subspace spanned by the first two singular vectors of the patch, i.e. its first two dipolar components shown by the plots of V_1 and V_2 in figure 8. For extremely focal sources (e.g. 5×5 mm), a rank two current dipolar model is sufficient, because these vectors explain 99% of the total source energy ($k = 2$). For more spatially extended sources, however, source models of higher dimension are required. Simulating such sources via 2D and 3D clusters of dipoles and comparing using subspace angles shows the ability of multipolar models to approximate the higher order subspaces obtained. This correspondence between model and cluster provides strong evidence for the claim that multipolar expansions are better suited to model spatially extended activation areas in MEG.

Finally, we note that these results were obtained with rather simplistic clusters of dipoles in a noiseless simulation, in order to highlight the relationship between current patterns, source size and multipolar models. We have begun investigations using realistic cortical grids of dipoles based on high-resolution brain segmentations. In Mosher *et al* (1999a), we showed how roughly 3.5 cm^2 cortical patches arbitrarily located anywhere in the cortical regions yielded MEG fields that were in many cases dipolar, and we repeated these observations for the EEG case in Mosher *et al* (1999b). Both cases were also computed in substantial simulated noise. A smaller set of sources in these simulations did require the addition of the quadrupolar components, and further work is needed to quantify under what realistic conditions these models apply.

7. Discussion

The multipolar expansions derived in this paper are based on expansions of the scalar Green's function. The derivations lead to compact formulations of infinite series expansions in spherical coordinates and to Cartesian expansions about arbitrary locations in explicit forms for the first terms of the expansion (dipole and quadrupole). In this paper we also highlight the links between much of the early development in MEG/MCG current multipole expansions, the related expansions in magnetic multipoles, and recent work by ourselves and others in multipolar expansions applied to EEG and MEG.

Spherical harmonic and Cartesian magnetic and current multipole expansion methods have been described in this paper. Since all ultimately represent the same sources, they are, in principle, equivalent. A 'good' source model is one that describes the external field as accurately as possible in a parsimonious fashion. For MEG applications, the sources are expected to consist of groups of neurons in an extended region of cortex that is small compared to its total surface area. Since the number of multipolar terms required to achieve a given accuracy is roughly determined by the extent of the source and the relative distance from the expansion point to the source and the measurement region, it appears preferable to compute expansions about a location close to geometric centroid of the source. Just as current dipole

models involve the estimation of location and moment parameters, so inverse methods using first-order multipoles could involve estimation of the best expansion point and the source moments. The degree to which the best expansion point matches the centroid of the activated region and the accuracy with which this can be estimated in the presence of noise, remain open questions.

To date, the application of multipolar expansions to MEG source modelling has been impeded by the apparent complexity and variety of possible multipole expansion procedures on the one hand and by little evidence of the real utility of higher order models on the other. The fundamentals of the multipole expansions and their relationships, as presented in the this paper, may help to resolve the first of these issues. The cluster analysis that we have performed provides strong empirical support for the use of multipole models for representing extended sources in MEG. Future work will concentrate on the development and evaluation of methods for incorporating multipolar models in robust inverse procedures for MEG data analysis.

Acknowledgments

We thank Dr. Guido Nolte, at the University of New Mexico, for his helpful discussions in the revisions of the manuscript. This work was supported by the National Institute of Mental Health Grant RO1-MH53213, the National Foundation from Functional Brain Imaging in Albuquerque NM and by Los Alamos National Laboratory, operated by the University of California for the United States Department of Energy under contract W-7405-ENG-36.

Appendix A. Deriving curl of $\mathbf{A}^p$

Using $\nabla \times (V\boldsymbol{U}) = \nabla V \times \boldsymbol{U} + V\nabla \times \boldsymbol{U}$, we perform the curl on the first term in (41),

$$\nabla \times \left(\frac{\boldsymbol{q}}{|\boldsymbol{r}-\boldsymbol{l}|} \right) = -\frac{(\boldsymbol{r}-\boldsymbol{l})}{|\boldsymbol{r}-\boldsymbol{l}|^3} \times \boldsymbol{q} = \boldsymbol{q} \times \frac{(\boldsymbol{r}-\boldsymbol{l})}{|\boldsymbol{r}-\boldsymbol{l}|^3} \,.$$

The curl in the second term of (41) yields

$$\nabla \times \left(\frac{(\boldsymbol{r}-\boldsymbol{l}) \cdot \tilde{\boldsymbol{Q}}_E}{|\boldsymbol{r}-\boldsymbol{l}|^3} \right) = \frac{-3(\boldsymbol{r}-\boldsymbol{l})}{|\boldsymbol{r}-\boldsymbol{l}|^5} \times ((\boldsymbol{r}-\boldsymbol{l}) \cdot \tilde{\boldsymbol{Q}}_E) + \frac{\nabla \times \left[(\boldsymbol{r}-\boldsymbol{l}) \cdot \tilde{\boldsymbol{Q}}_E \right]}{|\boldsymbol{r}-\boldsymbol{l}|^3}$$

where

$$\begin{aligned}
\nabla \times \left[(\boldsymbol{r}-\boldsymbol{l}) \cdot \tilde{\boldsymbol{Q}}_E \right] &= \int \nabla \times ((\boldsymbol{r}-\boldsymbol{l}) \cdot (\boldsymbol{r}'-\boldsymbol{l})\, \boldsymbol{J}^p(\boldsymbol{r}'))\, \mathrm{d}^3 r' \\
&= \int \nabla((\boldsymbol{r}-\boldsymbol{l}) \cdot (\boldsymbol{r}'-\boldsymbol{l})) \times \boldsymbol{J}^p(\boldsymbol{r}')\, \mathrm{d}^3 r' \\
&= \int ((\boldsymbol{r}'-\boldsymbol{l}) \cdot \nabla)(\boldsymbol{r}-\boldsymbol{l}) \times \boldsymbol{J}^p(\boldsymbol{r}')\, \mathrm{d}^3 r' \\
&= \int (\boldsymbol{r}'-\boldsymbol{l}) \times \boldsymbol{J}^p(\boldsymbol{r}')\, \mathrm{d}^3 r' \\
&= 2\,\boldsymbol{m}^p - \boldsymbol{l} \times \boldsymbol{q} \qquad \text{(A.1)}
\end{aligned}$$

where $\boldsymbol{m}^p$ is the *primary* magnetic dipole defined in (43). Performing the appropriate substitutions in (41) yields (42).

Appendix B. Solution to Poisson equation for $\boldsymbol{r} \cdot \boldsymbol{B}$

Beginning with (93), standard vector identities yield

$$a = \frac{\mu_0}{4\pi} \int \frac{\boldsymbol{J}(\boldsymbol{r}') \times (\boldsymbol{r}-\boldsymbol{r}')}{|\boldsymbol{r}-\boldsymbol{r}'|^3} \cdot \boldsymbol{r}\, \mathrm{d}^3 r' = \frac{\mu_0}{4\pi} \int \frac{\boldsymbol{J}(\boldsymbol{r}') \cdot (\boldsymbol{r}-\boldsymbol{r}')}{|\boldsymbol{r}-\boldsymbol{r}'|^3} \times \boldsymbol{r}\, \mathrm{d}^3 r'. \qquad \text{(B.1)}$$

Using the identity

$$(\boldsymbol{r} - \boldsymbol{r}') \times \boldsymbol{r} \;=\; \boldsymbol{r} \times \boldsymbol{r}' \;=\; (\boldsymbol{r} - \boldsymbol{r}') \times \boldsymbol{r}' \tag{B.2}$$

(B.1) can be written as

$$= \frac{\mu_0}{4\pi} \int \frac{\boldsymbol{J}(\boldsymbol{r}') \cdot (\boldsymbol{r} - \boldsymbol{r}')}{|\boldsymbol{r} - \boldsymbol{r}'|^3} \times \boldsymbol{r}' \, \mathrm{d}^3 r'$$

yielding (96). Starting with (93), the same result (96) is thus obtained through simple vector calculus. The rather unobvious relationship between (93) and (96) is best understood by considering the implications of the identity in (B.2).

References

Alvarez R E 1991 Filter functions for computing multipole moments from the magnetic field normal to a plane *IEEE Trans. Med. Imag.* **10** 375–81

Bouwkamp C J and Casilmir H B G 1954 On multipole expansions in the theory of electromagnetic radiation *Physica* **20** 539–54

Bronzan J B 1971 The magnetic scalar potential *Am. J. Phys.* **39** 1357–9

Bronzan J B 1982 Magnetic scalar potentials and the multipole expansion for magnetostatics *Electromagnetism: Paths to Research* ed D Teplitz (New York: Plenum) 5 pp 171–81

Burghoff M, Nenonen J, Trahms L and Katila T 2000 Conversion of magnetocardiographic recordings between two different multichannel SQUID devices *IEEE Trans. Biomed. Eng.* **47** 869–75

Burghoff M, Steinhoff U, Haberkorn W and Koch H 1997 Comparability of measurement results obtained with multi-SQUID-systems of different sensor configurations *IEEE Trans. Appl. Supercond.* **7** 3465–8

Castellanos A, Panizo M and Rivas J 1978 Magnetostatic multipoles in Cartesian coordinates *Am. J. Phys.* **46** 1116–7

de Munck J C, van Dijk B W and Spekreijse H 1988 Mathematical dipoles are adequate to describe realistic generators of human brain activity *IEEE Trans. Biomed. Eng.* **35** 960–6

Ernè S N, Trahms L and Trontelj Z 1988 Current multipoles as sources of biomagnetic fields *Biomagnetism '87* ed K Atsumi *et al* (Tokyo: Denki University Press) pp 302–5

Geselowitz D B 1965 Two theorems concerning the quadrupole applicable to electrocadiography *IEEE Trans. Biomed. Eng.* **12** 164

Geselowitz D B 1970 On the magnetic field generated outside an inhomogeneous volume conductor by internal current sources *IEEE Trans. Magn.* **6** 346–7

Golub G H and van Loan C F 1989 *Matrix Computations* (Baltimore, MD: Johns Hopkins University Press)

Gonnelli R S and Agnello M 1987 Inverse problem solution in cardiomagnetism using a current multipole expansion of the primary sources *Phys. Med. Biol.* **32** 133–42

Gonzalez H, Juarez S R, Kielanowski P and Loewe M 1998 Multipole expansion in magnetostatics *Am. J. Phys.* **66** 228–31

Gray C G 1978 Simplified derivation of the magnetostatic multipole expansion using the scalar potential *Am. J. Phys.* **46** 582–3

Gray C G 1979 Magnetic multipole expansions using the scalar potential *Am. J. Phys.* **47** 457–9

Gray C G 1980 Definition of the magnetic quadrupole moment *Am. J. Phys.* **48** 984–5

Grynszpan F and Geselowitz D B 1973 Model studies of the magnetocardiogram *Biophys. J.* **13** 911–25

Haberkorn W 1994 Effekte des Volumenleiters auf biomagnetische Multipolfelder *Biomed. Technik* **39** 117–8

Haberkorn W 1998 Biomagnetic inverse solutions in terms of multipoles *Studies in Applied Electromagnetics and Mechanics* **13** ed V Kose and J Sievert (Amsterdam: IOS Press) pp 29–32

Hämäläinen M, Hari R, Illmoniemi R J, Knuutila J and Lounasmaa O V 1993 Magnetoencephalography—theory, instrumentation, and applications to invasive studies of the working human brain *Reviews of Modern Physics* **65** 413–98

Jackson J D 1975 *Classical Electrodynamics* (New York: Wiley)

Karp P J, Katila T E, Saarinen M, Siltanen P and Varpula T 1980 The normal human magnetocardiogram, II. A multipole analysis *Circ. Res.* **47** 117–30

Katila T E 1983 On the current multipole presentation of the primary current distributions *Il Nuovo Cimento* **2D** 660–4

Katila T E and Karp P 1983 Magnetocardiography: Morphology and multipole presentations *Biomagnetism: An Interdisciplinary Approach* (New York: Plenum) pp 237–63

Morse P M and Feshbach H 1953 *Methods of Theoretical Physics, Part II* (New York: McGraw-Hill)

Mosher J C, Baillet S, Jerbi K and Leahy R M 2000 MEG Multipolar Modeling of Distributed Sources Using RAP-MUSIC *Conf. Record of the Thirty-Fourth Asilomar Conf. on Signals, Systems and Computers* **1** 318–22

Mosher J C, Baillet S and Leahy R M 1999b EEG Source Localization and Imaging Using Multiple Signal Classification Approaches *J. Clin. Neurophysiol.* **16** 225–38

Mosher J C, Leahy R M, Schattuck D and Baillet S 1999a MEG Source Imaging Using Multipolar Expansions *(Lecture Notes in Computer Science)* (Berlin: Springer) pp 98–111

Mosher J C, Lewis P S and Leahy R M 1992 Multiple dipole modeling and localization from spatiotemporal MEG data *IEEE Trans. Biomed. Eng.* **39** 541–57

Nenonen J, Katila T, Leiniö M, Montonen J, Mäkijärvi and Siltanen P 1991 Magnetocardiographic functional localization using current multipole models *IEEE Trans. Biomed. Eng.* **38** 648–57

Nolte G and Curio G 1997 On the calculation of magnetic fields based on multipole modeling of focal biological current sources *Biophys. J.* **73** 1253–62

Nolte G and Curio G 1999 Perturbative analytical solutions of the electric forward problem for realistic volume conductors *J. Appl. Phys.* **86** 2800–11

Nolte G and Curio G 2000 Current multipole expansion to estimate lateral extent of neural activity: a theoretical analysis *IEEE Trans. Biomed. Eng.* **47** 1347–55

Nolte G, Fieseler T and Curio G 2001 Perturbative analytical solutions of the magnetic forward problem for realistic volume conductors *J. Appl. Phys.* **89** 2360–9

Purcell C, Mashiko T, Odaka K and Ueno K 2000 Describing head shape with harmonic expansion *IEEE Trans. Biomed. Eng.* **38** 303–6

Sarvas J 1987 Basic mathematical and electromagnetic concepts of the biomagnetic inverse problem *Phys. Med. Biol.* **32** 11–22

Stroink G 1987 Inverse problem solution in magnetisation studies *Phys. Med. Biol.* **32** 53–8

Wang J Z, Williamson S J and Kaufman L 1992 Magnetic source images determined by a lead-firel analysis: The unique minimum-norm least-squares estimation *IEEE Trans. Biomed. Eng.* **39** 665–75

Wikswo J P 1983 Theoretical aspects of the ECG-MCG relationship *Biomagnetism: An Interdisciplinary Approach* (New York: Plenum) pp 311–27

Wikswo J P and Swinney K R 1984 A comparison of scalar multipole expansions *J. Appl. Phys.* **56** 3039-49

Wikswo J P and Swinney K R 1985 Scalar multipole expansions and their dipole equivalence *J. Appl. Phys.* **57** 4301–8